

## Field Implementation and Monitoring of Bridge Approach Slabs

FINAL REPORT

August 2007

Submitted by

Hani Nassif<sup>1</sup>  
Associate Professor

Nakin Suksawang<sup>2</sup>  
Assistant Professor  
Talat Abu-Amra<sup>3</sup>  
Assistant Professor

Nirali Shah<sup>1</sup>  
Research Assistant

<sup>1</sup>Dept. of Civil & Environmental Engineering  
Department of Civil and Environmental Engineering  
Rutgers, The State University  
Piscataway, NJ 08854-8014

<sup>2</sup>Dept. of Civil & Environmental Engineering  
Florida International University  
Miami, FL

<sup>3</sup>Dept. of Civil, Construction and Environmental  
Engineering  
University of Alabama at Birmingham  
Birmingham, AL 35294



NJDOT Research Project Manager  
W. Lad Szalaj

In cooperation with

New Jersey  
Department of Transportation  
Bureau of Research  
And  
U. S. Department of Transportation  
Federal Highway Administration

## **Disclaimer Statement**

"The contents of this report reflect the views of the author(s) who is (are) responsible for the facts and the accuracy of the data presented herein. The contents do not necessarily reflect the official views or policies of the New Jersey Department of Transportation or the Federal Highway Administration. This report does not constitute a standard, specification, or regulation."

This document is disseminated under the sponsorship of the Department of Transportation, University Transportation Centers Program, in the interest of information exchange. The U.S. Government assumes no liability for the contents or use thereof.

1. Report No. <b>FHWA-NJ-2007-012</b>	2. Government Accession No.	3. Recipient's Catalog No.	
4. Title and Subtitle <b>FIELD IMPLEMENTATION AND MONITORING OF BRIDGE APPROACH SLABS</b>		5. Report Date <b>August 2007</b>	
		6. Performing Organization Code <b>Rutgers University</b>	
7. Author(s) <b>Hani Nassif, Nakin Suksawang, Nirali Shah, and Talat Abu-Amra</b>		8. Performing Organization Report No. <b>FHWA-NJ-2007-012</b>	
9. Performing Organization Name and Address <b>New Jersey Department of Transportation CN 600 Trenton, NJ 08625</b>		10. Work Unit No.	
		11. Contract or Grant No.	
		13. Type of Report and Period Covered <b>Final Report</b>	
12. Sponsoring Agency Name and Address <b>Federal Highway Administration U.S. Department of Transportation Washington, D.C.</b>		14. Sponsoring Agency Code	
15. Supplementary Notes			
16. Abstract  <p>Bridge approach slabs are designed to function as a transitional roadway to the bridge deck spanning the distance between the abutment and road pavement. However, the number of rough-riding approaches with heavy maintenance requirements is sufficient to convince highway agencies that a serious problem exists. The objective of this study is to implement and evaluate proposed design alternatives for bridge approach slabs under field conditions. Two design alternatives, Embedded Beam (EB) and Constant Thickness (CT), are implemented in the Doremus Avenue Bridge project. The study includes installation of sensors at various locations in bridge projects under contract and to verify the findings of the Phase I probable causes of cracking, location of cracks, factors influencing crack development, and to recommend new design alternative that could reduce or eliminate crack development in approach slabs. A field study is conducted and data is collected from field observations. Measured results were compared with those predicted by the finite element model to determine the reliability and the consistency of the model. Subsequently, several design alternatives were studied and compared to determine their effectiveness in reducing the possibility of crack development and tolerating higher vehicular loads. The embedded beam (EB) is recommended based on results from field observations and long term monitoring of their performance under normal traffic and environmental conditions. The new EB design alternative is adopted by the New Jersey Department of Transportation (NJDOT) as the detail for future use in the design of approach slabs.</p>			
17. Key Words <b>Approach Slab, Monitoring, Cracks, Finite Element Method, Instrumentation</b>		18. Distribution Statement	
19. Security Classif (of this report) <b>Unclassified</b>	20. Security Classif. (of this page) <b>Unclassified</b>	21. Total pages <b>86</b>	22. Price

## **ACKNOWLEDGEMENTS**

The authors would like to thank the New Jersey Department of Transportation (NJDOT) and staff for their help and support of this project: W. Lad Szalaj, NJDOT project manager, Jose Lopez, Nick Vittilo (retired), Harry Capers, Jr. (retired), and Richard Dunne, for their help and assistance throughout the project. Also, the help of the Slattery-Skanska (Contractor for the Doremus Avenue Bridge Project) for their accommodations is appreciated. The authors would like to acknowledge the help and work of former graduate students, Kedar Redkar, Yasser Khodair, and William Cao on this topic.

## TABLE OF CONTENTS

SUMMARY .....	1
INTRODUCTION.....	1
OBJECTIVE .....	2
DESIGN ALTERNATIVES.....	2
FINITE ELEMENT MODEL OF NEW APPROACH SLAB DESIGNS .....	4
FIELD INSTRUMENTATION AND TESTING PROGRAM .....	6
Visual Inspection of Soil Strata.....	6
Grain Size Distribution of Filled Soil.....	7
Location of Sensors .....	7
Vibrating Wire Strain Gages:(Model 4200).....	15
Soil Strain Meter (Model 4430).....	16
"Fat Back" Pressure Cell (Model 4810).....	18
Settlement Sensor (Model 4650).....	20
Installation of Sensors and WIM System .....	22
VWSG .....	22
VW Deformation Meter.....	22
Pressure Cell.....	22
Settlement Sensor.....	22
Data Logger .....	26
Weigh-In-Motion (WIM) System Installation .....	27
Concreting of Approach Slabs .....	29
Concreting Sequence.....	29
Typical Concrete Pour of Approach Slab .....	29
Sampling .....	30
Testing .....	31
STATIC TESTING.....	33
Test Truck Information and Testing Procedure .....	33
Results from Available Sensor Data .....	47
VWSG Results from NA-LN-3. ....	48
VWSG Results from NA-LN-4. ....	52
VWSG Results from SA-LN-3. ....	57
VWSG Results from SA-LN-4. ....	62
LONG-TERM MONITORING .....	69
CONCLUSIONS.....	73
RECOMMENDATIONS .....	73
REFERENCES.....	74
APPENDIX A.....	76

## LIST OF FIGURES

Figure 1. Layout of Approach Slabs on the Doremus Avenue Bridge. ....	3
Figure 2. 3-D FE model of the approach slab; (a) plan view and (b) isometric view. ....	5
Figure 3. Approach Slab area to be filled with Soil. ....	6
Figure 4. Grain Size Distribution Curve obtained from Sieve Analysis. ....	7
Figure 5. Critical Area for Sensors in Approach Slabs. ....	8
Figure 6. Location of Sensors for SA-LN-4. ....	9
Figure 7. Location of Sensors for SA-LN-3. ....	10
Figure 8. Location of Sensors for NA-LN-4. ....	11
Figure 9. Location of Sensors for NA-LN-3. ....	12
Figure 10. Notations for all types of sensors. ....	13
Figure 11. Picture and working mechanism of VWSG. ....	16
Figure 12. Picture and working mechanism of VW Deformation Meter. ....	17
Figure 13. Picture and working mechanism of Pressure Cell. ....	19
Figure 14. Picture and working mechanism of Settlement Sensor. ....	21
Figure 15. VWSG Connected to Wires Ready for Delivery and Installation on Site. ....	23
Figure 16. VWSG installed Longitudinally and Transversely at Site. ....	23
Figure 17. (a) Embedded and (b) grouted VW Deformation Meter. ....	24
Figure 18. Pressure Cell installed underneath Approach Slab near the VW Deformation Meter. ....	25
Figure 19. Settlement Sensor installed in Soil strata underneath Approach Slab. ....	25
Figure 20. Data logger box and Solar Panel installed on wing wall. ....	26
Figure 21. Downloading Data from Data-Logger Using Portable Computer. ....	26
Figure 22. Bending Plate Fixed WIM System Installed on SA-LN-3 and SA-LN-4. ....	27
Figure 23. Conduits laid for WIM System Installation at South Abutment. ....	28
Figure 24. Bending Plate WIM System with Loop Detectors installed at the South Abutment. ....	28
Figure 25. Concrete pouring sequence of approach slabs on the Doremus Avenue Bridge. ....	29
Figure 26. Concreting of Approach Slab for Concrete Pour No. 1. ....	30
Figure 27. Concrete Cylinders Cured on Site using Burlap. ....	31
Figure 28. Comparison of Compressive Strengths for Concrete Pour-2. ....	32
Figure 29. Experimental Setup for testing the Elastic Modulus of Concrete. ....	32
Figure 30. Comparison of Elastic Modulus for two slabs of Concrete Pour No. 2. ....	33
Figure 31. Various Truck Positions for Static Load Testing of new Approach Slabs. ....	34
Figure 32. Shrinkage in Concrete Structures. ....	48
Figure 33. Shrinkage plots for sensors along edge towards Lane-4. (NA-LN-3) (From-10/24/02-03/14/03) ....	49

Figure 34. Plots of shrinkage for sensors in the middle of the lane, NA-LN-3 (From-11/01/02-03/14/03) .....	50
Figure 35. Plots of shrinkage for all transverse sensors, NA-LN-3. (From-10/24/02-03/14/03) .....	51
Figure 36. Shrinkage plots for sensors along edge towards shoulder (NA-LN-4). (From-11/01/02-03/14/03) .....	53
Figure 37. Shrinkage plots for sensors along edge towards NA-LN-3. (NA-LN-4). (From-11/01/02-03/14/03) .....	54
Figure 38. Plots of shrinkage for sensors in the middle of the lane, NA-LN-4 (From-11/01/02-03/14/03) .....	55
Figure 39. Plots of shrinkage for all transverse sensors, NA-LN-4. (From-10/24/02-03/14/03) .....	56
Figure 40. Shrinkage Plots for Edge Sensors towards SA-LN-4. (SA-LN-3) (From-10/24/02-03/14/03) .....	58
Figure 41. Shrinkage plots for sensors along edge away from SA-LN-4. (SA-LN-3) (From-10/24/02-03/14/03) .....	59
Figure 42. Plots of shrinkage for sensors in the middle of the lane, SA-LN-3 (From-11/01/02-03/14/03) .....	60
Figure 43. Shrinkage plots for all transverse sensors, SA-LN-3. (From-11/01/02-03/14/03) .....	61
Figure 44. Shrinkage plots for sensors along edge towards shoulder. (SA-LN-4). (From-10/24/02-03/14/03) .....	63
Figure 45. Shrinkage plots for sensors along edge towards SA-LN-3. (SA-LN-4). (From-10/24/02-03/14/03) .....	64
Figure 46. Plots of shrinkage for sensors in the middle of the lane, SA-LN-4. (From-10/24/02-03/14/03) .....	65
Figure 47. Shrinkage plots for transverse sensors, SA-LN-4. (From-10/24/02-03/14/03) .....	66
Figure 48. Plots of VW Deformation Meter for SA-LN-3. (From-11/01/02-12/31/02) .....	67
Figure 49. Plots for pressure cell data. (NALN-4 and SA-LN-3) (From-11/01/02-12/31/02) .....	68
Figure 50. Typical Strain Readings of the EB and CT slabs in the North Abutment.....	69
Figure 51. Typical Strain Readings of the EB and CT slabs in the South Abutment.....	70
Figure 52. Crack Location and orientation in new Approach Slab at the Doremus Avenue Bridge .....	70
Figure 53. Strain and temperature profile at crack location. ....	71
Figure 54. Typical strain and temperature profile of approach slabs.....	72
Figure 55. Typical displacement and pressure profile of approach slabs.....	72
Figure 56. Detail of Existing Design of Approach Slabs.....	76
Figure 57. Detail of Existing Design of Transition Slabs.....	77
Figure 58. Detail of the EB Approach Slabs Adopted by NJDOT .....	78

## LIST OF TABLES

Table 1. Cracking Load for 45 ft and 55 ft Approach Slabs. ....	6
Table 2. Exact location of sensors in all slabs. ....	13
Table 3. Specifications for Vibrating Wire Strain Gages (VWSG) .....	15
Table 4. Specifications for VW Deformation Meter. (Manual). ....	17
Table 5. Specifications of "Fat Back" Pressure Cell (Model 4810) (Manual) .....	18
Table 6. Specifications for Settlement Sensor, Model 4650. ....	20
Table 7. Information of Truck, used for Approach Slab Testing. ....	35
Table 8. Comparison of the finite element results and the field results for NA-LN-3. ....	36
Table 9. Comparison of Results for the finite element and the field tests for SA-LN-3. ....	40
Table 10. Comparison of the finite element results and the field results for SA-LN-4. ....	44



### FIGURES NOTATION

A	Approach slab
A/T	Approach and Transition Slab
F	Front Axle (8 kips)
m	Distance of cracked element from SIDE D
M	Middle Axle (32 kips)
n	Distance of cracked element from SIDE D
R	Rear Axle (32 kips)
T	Transition slab
W	Wing wall
x	Distance of cracked element from SIDE B
y	Distance of cracked element from SIDE B

### EQUATIONS NOTATION

a	Effective moment arm
$A_s$	Area of Steel
b	Width of concrete section
d	Effective depth of concrete section
$f'_c$	Compressive strength of Concrete
$F_y$	Yield strength of steel
L	Span length
$l_n$	Effective span length
$M_n$	Nominal moment
$M_u$	Ultimate moment
P	Wheel load
S	Spacing between beams
$S_h$	Maximum permissible spacing between horizontal bars
$S_v$	Maximum permissible spacing between vertical bars
w	Dead load
f	Load factor

## SUMMARY

Bridge approach slab is a concrete transitional roadway between the bridge deck and the asphalt pavement. It is designed to reduce the vehicle dynamic effects on the bridge. However, growing numbers of rough riding and cracked approach slabs with heavy maintenance requirements is sufficient to convince highway agencies that a serious problem exists. The complaints usually describe a 'bump' that motorists feel when they approach or leave bridges. This bump results in reduction of steering response, distraction to the driver, amplified truck impact and dynamic response in bridge decks, and expense to maintenance operations. As a result, the approach slabs can lose their contact supports due to various reasons, including the settlement of soil and the bulging of embankments. Together with the increasing truck load spectra, the approach slab will eventually crack despite the proper compaction made prior to the construction of the approach slabs. Therefore, alternative approach slab designs need to be investigated to solve the rough riding and cracks in approach slabs.

Two new design alternatives, embedded beam (EB) and constant thickness (CT), are developed and optimized during the Phase I of this study using advanced finite element program, ABAQUS.<sup>(1,2,3)</sup> The two design alternatives were recommended for implementation on the newly constructed Doremus Avenue Bridge to determine and monitor their effectiveness under field conditions. The transition slab (see Appendix A), commonly used in New Jersey Department of Transportation (NJDOT) designs of the approach slabs, are eliminated from the two design alternatives so that they only have a constant thickness of 18 in. Additionally, top layer reinforcements are added to the design alternatives to restrain the concrete from cracking due to thermal stresses. Several approach slab lengths, 35 ft, 45 ft, and 55 ft are investigated to determine the optimum approach slab length. Based on static load tests and long-term monitoring of the EB and CT design alternatives, both design alternatives outperformed existing design used by NJDOT. The EB design alternative has the best performance and did not exhibit any cracks on the Doremus Avenue Bridge under normal truck traffic conditions or soil settlement. The 45 ft length was the optimum design length without increasing the cost of the approach slabs. Therefore, the embedded beam design is recommended and currently adopted by the NJDOT to be the future design standard for bridge approach slabs.

## INTRODUCTION

Approach slabs are used as transitional roadway between the pavement and the actual structure of the bridge to reduce the dynamic effects imposed on the bridge by heavy truckloads. More than 25% of bridges in the US are affected by problems associated with approach slabs.<sup>(4)</sup> The surface irregularities in approach slabs (i.e. bumps) affect both the traveling public and the highway maintenance organization. These bumps, dips, and cracks are unsafe and destructive to vehicles and bridge structures. This problem can be caused by the following: (1) settlement of soil, (2) poor fill material, (3)

inadequate compaction, (4) poor drainage, and (5) poor structural design of the approach slab. Despite the widespread occurrence of bridge approach problems, only a small number of research studies have been performed on the subject. Few studies have been developed for evaluating the cracking behavior of bridge approach slabs in particular. However, this problem is becoming an increasingly important topic in the effort to deal with the deteriorating infrastructure and rehabilitation of roadways. The disposition or repair of these deteriorating slabs involves clear financial and safety implications. To avoid high costs of replacement or repair, the evaluation must accurately reveal the present conditions and predict any further changes (or deterioration) in the applicable time span. Major decisions must be made to allocate the limited funds available for repair, rehabilitation, and/or replacement, on the basis of a detailed evaluation of the structural integrity of bridge approach slabs. Therefore, an efficient analytical model is needed for the prediction of the cracking behavior and the optimum design schemes in order to ensure crack free slabs. Moreover, it is important to understand the three-dimensional behavior of the slab-soil-vehicle interaction system. The effect of various parameters on the current design provisions used by NJDOT is studied in particular.

## **OBJECTIVE**

The objective of this research study is to recommend new design alternatives based on field-testing and evaluation of their performance under actual traffic conditions. The study includes:

- Implementation of newly developed design alternatives of approach slabs (Phase I) on the Doremus Avenue Bridge, NJ; the first bridge in NJ designed according to AASHTO LRFD.
- Instrumentation of newly constructed approach slabs with different types of sensors and evaluation of their performance based on field data.
- Recommend new design detail based on static testing and long-term monitoring of the slab performance under field conditions.

## **DESIGN ALTERNATIVES**

Three approach slabs, two new design alternatives designed and analyzed by the Rutgers Team in Phase I of this study (embedded beam (EB) and constant (CT)) as well as the existing NJDOT details, were constructed at the Doremus Avenue Bridge, located in Newark, New Jersey. Each approach slab design had three different lengths; 35 ft, 45 ft and 55 ft. During construction, the two design alternatives were instrumented with sensors, including vibrating wire strain gages (VWSG), settlement sensors, pressure cells, and deflection meter, to monitor their long-term performances. Figure 1 shows the layout of the new and existing approach slabs on the Doremus Avenue Bridge located in Newark, NJ. The Doremus Avenue Bridge is a four-lane bridge with two approach slabs at the North approach, in lanes 1 and 2, labeled NA-LN-1 and NA-LN-2, respectively, were already constructed according to the existing NJDOT design

details. It was suggested that the slabs in lanes 3 and 4 on the same North approach (labeled NA-LN-3 and NA-LN-4, respectively), should be constructed using the new design alternatives, EB and CT, respectively. The length of NA-LN-3 is 35 ft on the shorter side and 38 ft on the longer side, with an average of 36.5 ft, whereas that of NA-LN-4 is 38 ft on the shorter side and 41ft on the longer side, with an average of 39.5 ft. The South approach, lane 1 (SA-LN-1) and south approach, lane 2 (SA-LN-2) were constructed of EB and CT, respectively, both having a length of 55ft. Similarly, lanes 3 and 4 of the South approach (labeled SA-LN-3 and SA-LN-4, respectively) were constructed of EB and CT, respectively, both having a length of 45ft.

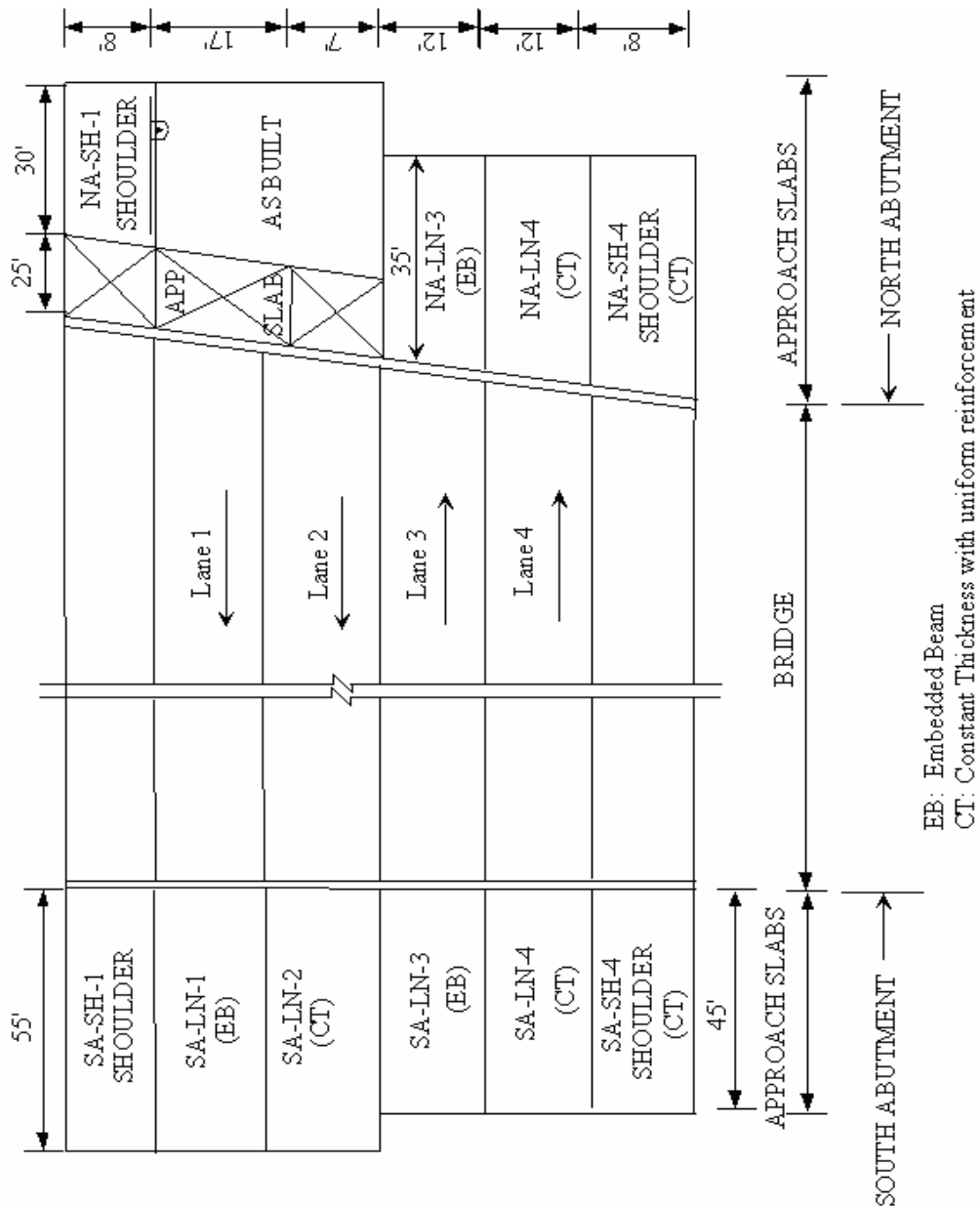


Figure 1. Layout of Approach Slabs on the Doremus Avenue Bridge.

## FINITE ELEMENT MODEL OF NEW APPROACH SLAB DESIGNS

A three dimensional (3-D) is developed in addition to the two-dimensional finite element (FE) model used in Phase I of the project.<sup>(1,2,3)</sup> Figures 2a and 2b illustrate the 3-D FE model of the approach slab. In the 3-D FE model, the soil and the slab are both modeled using eight-nodded solid continuum elements. The concrete slab is made of brick elements having a compressive strength of 5.8 ksi. The reinforcement is modeled using embedded membrane elements in the concrete to represent the rebar having a tensile ultimate strength of 70 ksi. Since the soil has an unbounded domain, two layers of soil are used. The top layer represents the compacted 3 ft sand and gravel soil modeled using “pour pressure” elements. The bottom layer simulated the embankment by using infinite eight-nodded elements. The slab is pinned at its connection with the abutment, while the rest of the slab is supported by soil. At the interface between the slab and the soil, a friction coefficient of 0.3 is assumed based on sieve analysis and soil profile obtained from the Doremus Avenue Bridge geotechnical data. This data shows that the soil underneath the approach slab is a fill material and extends to a depth of around 3 ft. A variety of materials including cinder, slag, plastic, and wood fragments are found within the fill in some areas. Soil below the filled portion extended to a depth of 30 ft. The soil used for backfilling is sand with granular materials, as well as some interlayer of silt and clay, and the top portion of the bottom layer is organic clay and silt. Moreover, the sieve analysis shows that the soil is gap graded.

Based on the soil information, standard soil properties from Das (1999) are used to determine the mechanical properties as follows: Modulus of elasticity value of 25 ksi for the top layer and 5 ksi for the bottom layer, Poison’s ratio of 0.35, permeability ( $k$ ) value of 0.004, specific weight value of 0.07 lb/in<sup>3</sup>, and void ratio value of 0.45 for the top layer and 1.4 for the bottom layer. A Mohr-Coulomb yield criterion is also used to model the fill behavior with an angle of internal friction of 35 degrees and a cohesion yield stress of 10 ksi.

The analysis is carried out in two steps: (1) the consolidation of the soil due to the dead load of the slab where drainage is allowed to occur in the soil and (2) the application of the truckload. In both (2-D and 3-D) FE models, the approach slabs are subjected to multiples of the HS-20 bridge design truck loading. The HS-20 truck has three axles: (1) 8 kips front axle weight, (2) 32 kips middle axle weight, and (3) 32 kips rear axle weight. The longitudinal and transverse spacing of the truck is 14 ft and 6 ft, respectively. The HS-20 truck is modeled as six point loads corresponding to the loads and spacing described above.

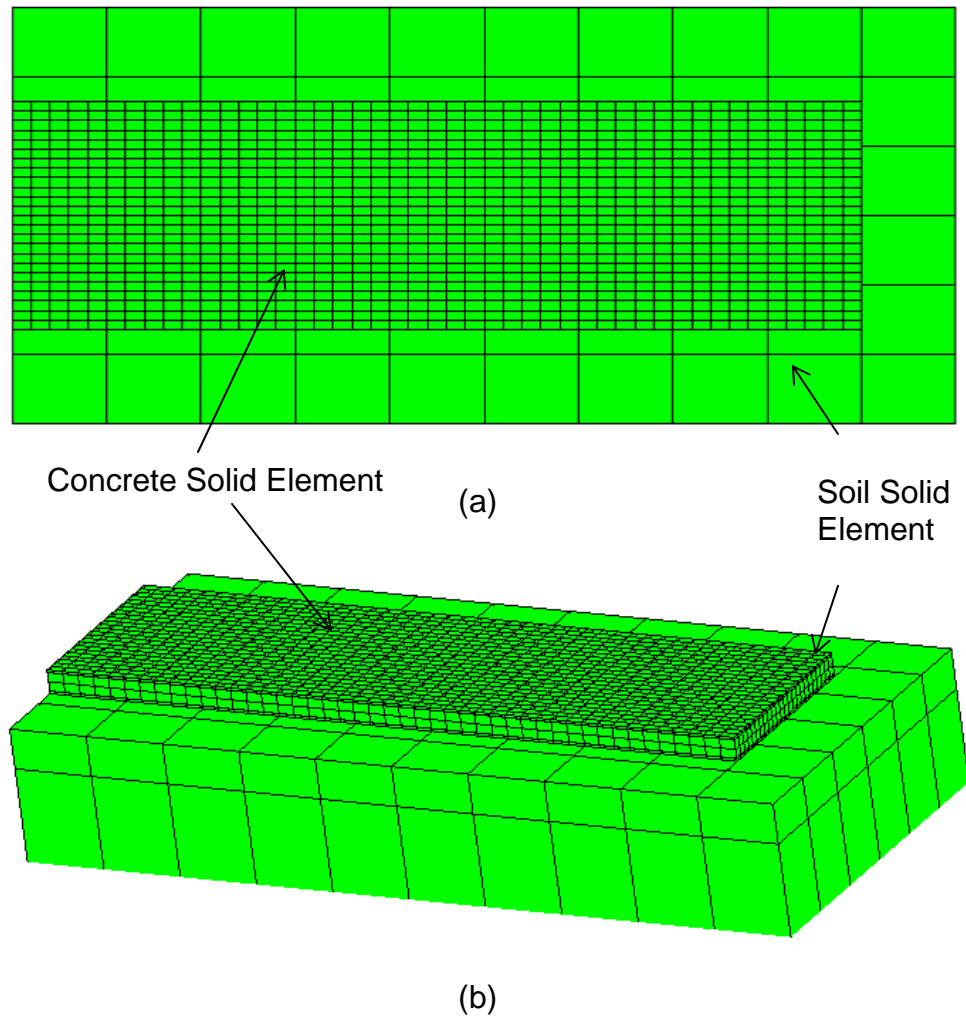


Figure 2. 3-D FE model of the approach slab; (a) plan view and (b) isometric view.

The 3D FE model is used to determine the sensors locations as well as to predict the load level at which the slab will undergo cracking. Table 1 shows the cracking load required for the first element to crack for 35 ft, 45 ft, and 55 ft slabs for both CT and EB designs. For both CT and EB designs, the 35 ft and 45 ft slightly outperformed the 55 ft with cracking loads of 4.5 times HS20 truck versus a cracking load of 4.3 times HS20 truck. The critical locations are also noted so that the sensors could be installed in the proximity of the cracked element predicted by the 3D FE model. For the both CT and EB approach slabs at any given length, the location where the approach will crack first is approximately 8 ft from the abutment.

Table 1. Cracking Load for 45 ft and 55 ft Approach Slabs.

	CT	EB
35 FT	4.5 Times HS 20	4.5 Times HS 20
45 FT	4.5 Times HS 20	4.5 Times HS 20
55 FT	4.3 Times HS 20	4.3 Times HS 20

## FIELD INSTRUMENTATION AND TESTING PROGRAM

### Visual Inspection of Soil Strata

The soil right under the approach slab is a fill material and extends to a depth of around 3.5-4 ft. Figure 3 depicts the area of the approach slab for Doremus Avenue Bridge, which is to be filled with soil as well as soil for filling stacked near the approach slab area. A variety of materials including cinder, slag, plastic and wood fragments are also found within the fill in some areas.

The soil below the filled portion extends to a depth of approximately 30ft. The soil used for backfilling is sand with granular materials as well as some interlayer of silt and clay, and the top portion of the bottom layer is organic clay and silt.



Figure 3. Approach Slab area to be filled with Soil.

## Grain Size Distribution of Filled Soil

Sieve analysis is performed in order to determine grain size distribution of the soil directly beneath the approach slabs. A sample of soil is taken in its loose state and is oven dried for 24 hrs. The oven-dried sample is passed through sieve No. 3/4, 1/2, 3/8, 4, 16, 30, 50, 100, and 200 respectively. Figure 4 shows a plot of percentage finer versus sieve size on a logarithmic scale. Soil is found to be gap graded and it is deficient in particular range of sizes.

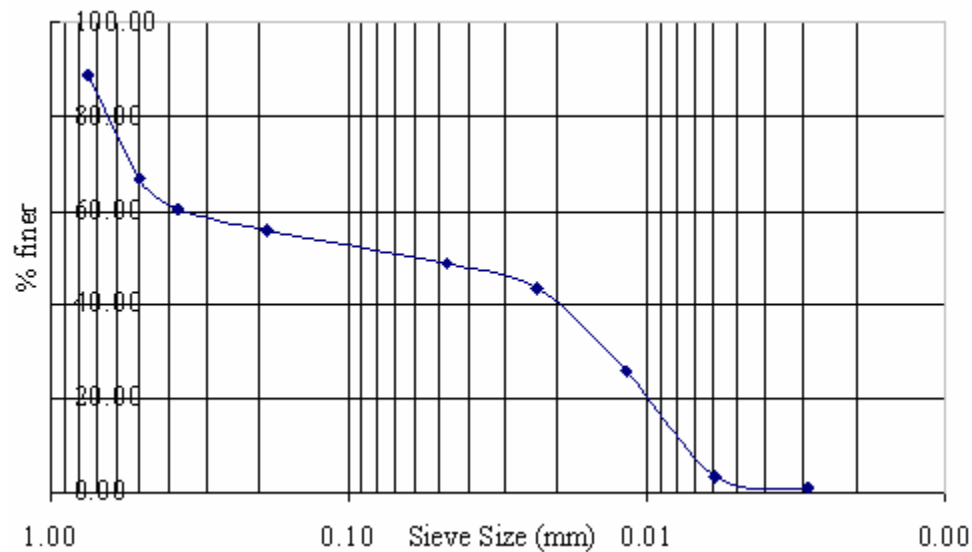


Figure 4. Grain Size Distribution Curve obtained from Sieve Analysis.

## Location of Sensors

In phase I of this study, it was observed that most of the cracks in the approach slabs are located near the abutment. Among these cracks, the majority is found in the slab portion within the wing wall area. Few cracks were found in the slab portion towards the pavement. Figure 5 illustrates the hatched portion in the part of the slab that is more likely to crack. Based on these observations combined with the results from the 3-D FE analyses, it is decided to provide more sensors in those portions during instrumentation of the approach slabs.



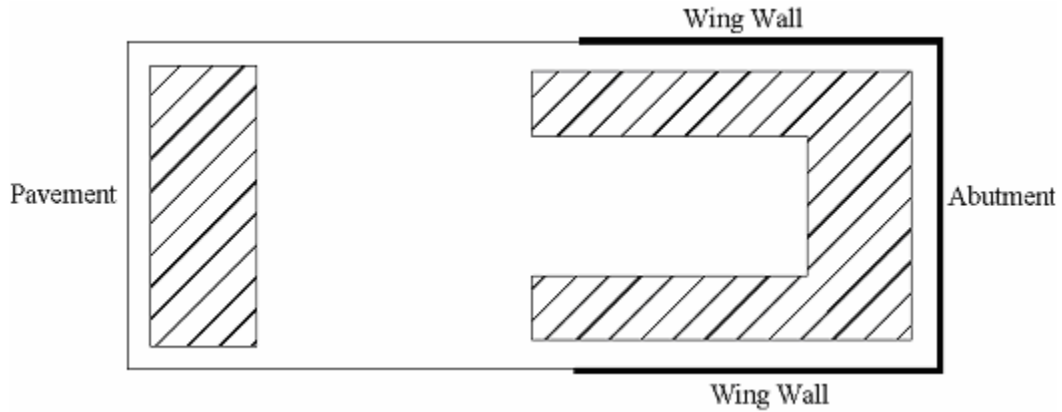


Figure 5. Critical Area for Sensors in Approach Slabs.

Each slab is instrumented with two typical patterns. Figure 6 through Figure 9 show the sensor types and locations instrumented in the approach slabs. Figure 10 shows the notations of sensors used for instrumentation of approach slabs. Table 2 illustrates the exact location of sensors in all slabs.

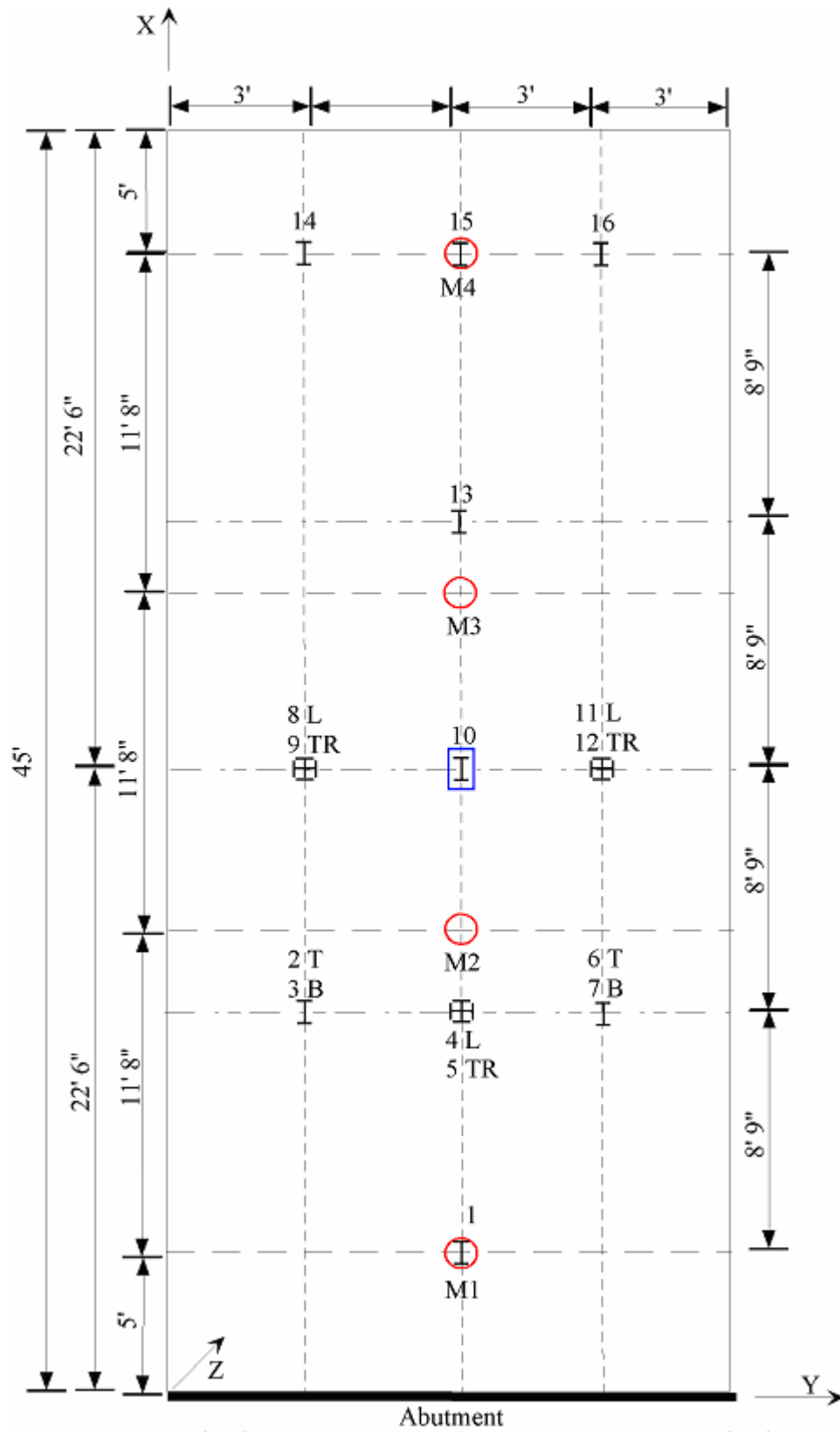


Figure 6. Location of Sensors for SA-LN-4.

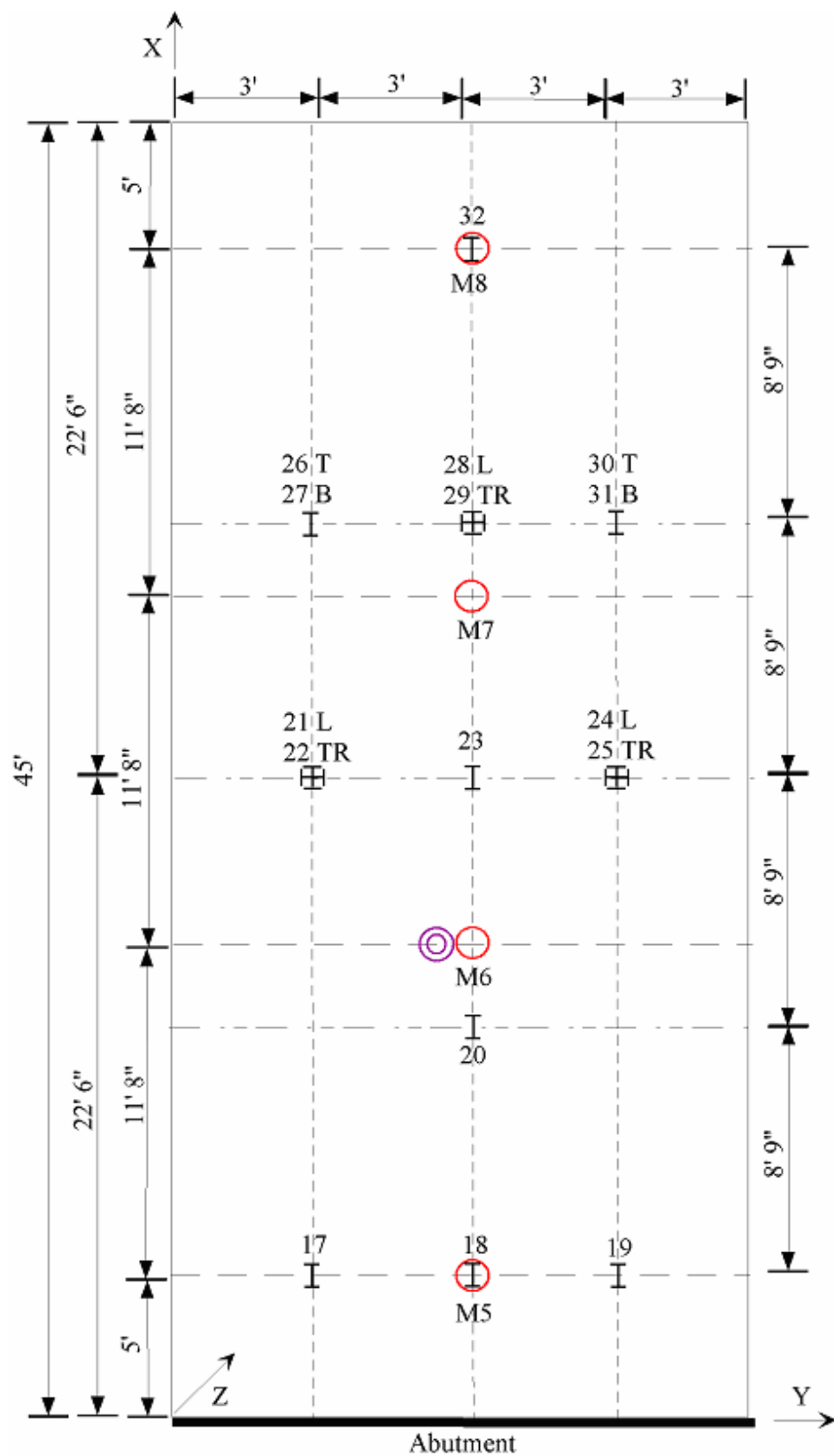


Figure 7. Location of Sensors for SA-LN-3.

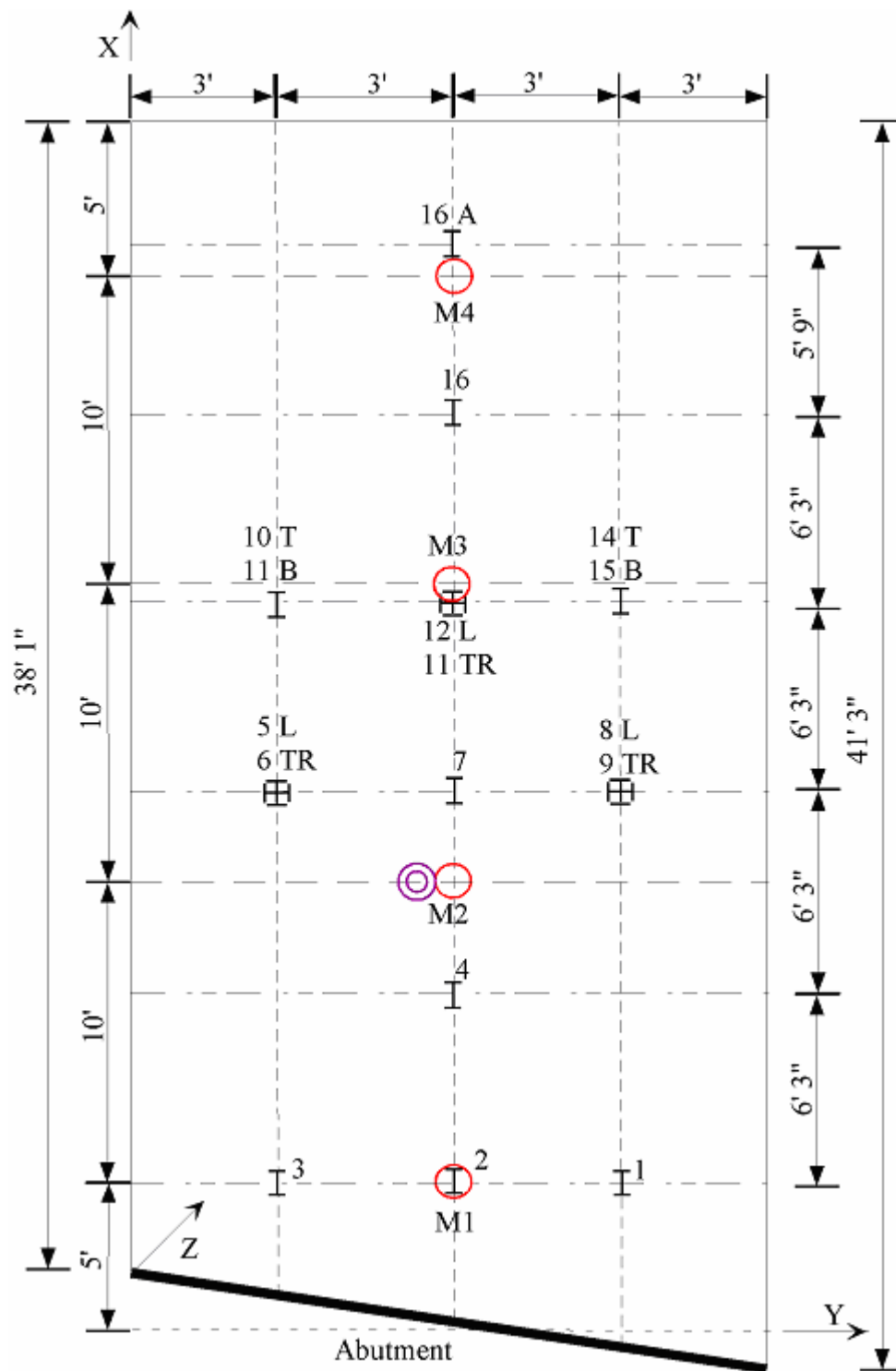


Figure 8. Location of Sensors for NA-LN-4.

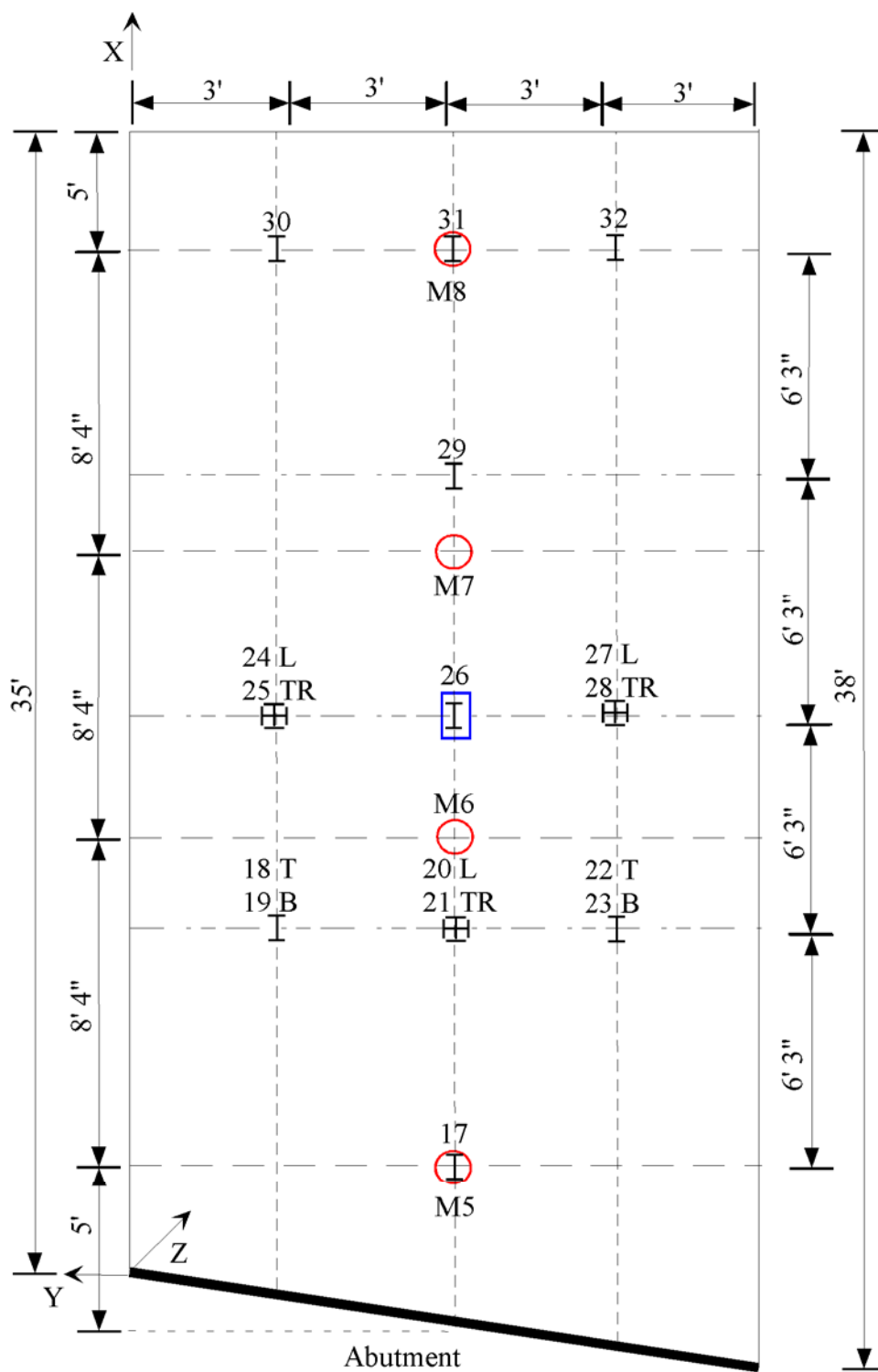


Figure 9. Location of Sensors for NA-LN-3.

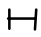



	Vibrating Wire Strain Gage
	Pressure Cell
	Settlement Sensor
	Vibrating Wire Deformation Meter

Figure 10. Notations for all types of sensors.

Table 2. Exact location of sensors in all slabs.

(a) SA-LN-4

Sensor No.	x	y	Z	Sensor No.	x	y	z
1	5' 3"	5' 7"	4.0"	12	22' 4"	5' 9"	4.0"
2	13' 3"	2' 8"	4.0"	13	31' 4"	5' 7"	4.0"
3	13' 3"	2' 8"	14.5"	14	40' 4"	8' 7"	4.0"
4	13' 3"	5' 9"	4.0"	15	40' 3"	5' 8"	4.0"
5	13' 3"	5' 9"	4.0"	16	40' 3"	2' 8"	4.0"
6	13' 3"	8' 7"	4.0"	M1	5'	6'	14"
7	13' 3"	8' 7"	14.5"	M2	16' 8"	6'	14"
8	22' 4"	2' 8"	4.0"	M3	28' 4"	6'	14"
9	22' 4"	2' 8"	4.0"	M4	40'	6'	14"
10	22' 4"	5' 8"	4.0"	ss	22' 6"	6'	18"
11	22' 4"	5' 8"	4.0"				

(b) SA-LN-3

Sensor No.	x	y	z	Sensor No.	x	y	z
17	4' 5"	3' 1"	4.0"	28	31'	6'	4.0"
18	4' 5"	6' 1"	4.0"	29	31'	6'	4.0"
19	4' 5"	9' 1"	4.0"	30	31'	3.0'	4.0"
20	14' 3"	6'	4.0"	31	31'	3.0'	14.5"
21	22' 3"	9.0'	4.0"	32	40' 2"	6'	4.0"
22	22' 3"	9.0'	4.0"	M5	5'	6'	14"
23	22' 3"	6'	4.0"	M6	16' 5"	6'	14"
24	22' 3"	3.0'	4.0"	M7	28' 2"	6'	14"
25	22' 3"	3.0'	4.0"	M8	40'	6'	14"
26	31'	9.0'	4.0"	P Cell	16' 9"	2' 9"	18"
27	31'	9.0'	14.5"				

Table (2) Exact location of sensors in all slabs (Continued)

(c) NA-LN-4

Sensor No.	x	y	z	Sensor No.	x	y	z
1	3' 8"	2' 10"	4.0"	12	23' 6"	5' 10"	4.0"
2	4' 7"	5' 11"	4.0"	13	23' 6"	5' 9"	4.0"
3	5' 3"	107"	4.0"	14	24' 4"	2' 10"	4.0"
4	11' 5"	5' 10"	4.0"	15	24' 4"	2' 10"	14.5"
5	16' 8"	8' 11"	4.0"	16	29' 6"	5' 9"	4.0"
6	16' 8"	8' 11"	4.0"	16A	35' 6"	5' 9"	4.0"
7	17' 5"	69"	4.0"	M1	5'	5' 8"	14"
8	18' 2"	2' 10"	4.0"	M2	15' 3"	5' 5"	14"
9	18' 2"	2' 10"	4.0"	M3	25'	6'	14"
10	22' 9"	8' 10"	4.0"	M4	35'	5' 8"	14"
11	22' 9"	8' 10"	14.5"	P. Cell	15' 3"	4' 9"	18"

(d) NA-LN-3

Sensor No.	x	y	z	Sensor No.	x	y	z
17	5'	6'	4.0"	28	17' 6"	2' 6"	4.0"
18	11' 3"	8' 11"	4.0"	29	23' 9"	5' 8"	4.0"
19	11' 3"	8' 11"	14.5"	30	30'	9'	4.0"
20	11' 3"	5' 7"	4.0"	31	30'	5' 8"	4.0"
21	11' 3"	5' 7"	4.0"	32	30'	2' 10"	4.0"
22	11' 3"	2' 7"	4.0"	M5	5'	6'	14"
23	11' 3"	2' 8"	14.5"	M6	13' 4"	6'	14"
24	17' 6"	8' 10"	4.0"	M7	21' 8"	6'	14"
25	17' 6"	8' 10"	4.0"	M8	30'	6'	14"
26	17' 6"	5' 8"	4.0"	SS	22' 6"	6'	18"
27	17' 6"	2' 6"	4.0"				

## Type of Sensors

Four different types of sensors are used for the instrumentation of the slab:

1. Vibrating Wire Strain Gage
2. Vibrating Wire Deformation Meter
3. Pressure Cell
4. Settlement Sensor

The specifications and working mechanism of each type of sensor are listed below:

### **Vibrating Wire Strain Gages:(Model 4200)**

The VWSGs are designed for direct embedment in concrete and are suitable for use in large aggregate concrete. Specifications for these types of gages are listed in Table 3. Figure 11(a) shows a picture of Vibrating Wire Strain Gage, Model 4200.

A length of steel wire is tensioned between two end blocks that are embedded directly in concrete. Deformations (i.e. strain changes) of the concrete mass will cause the two end blocks to move relative to each other, thus altering the tension in the steel wire. The tension is measured by plucking the wire and measuring its resonant frequency of vibration using an electromagnetic coil. The strain gages are provided with thermistors encapsulated in the plucking coil. The thermistor enables temperatures to be measured. A GK-403 readout Box is used to read strain data. It provides the necessary voltage pulses to pluck the wire and converts the resulting frequency reading directly into strain units by means of an internal microprocessor. Figure 11(b) illustrates the working mechanism of VWSG.

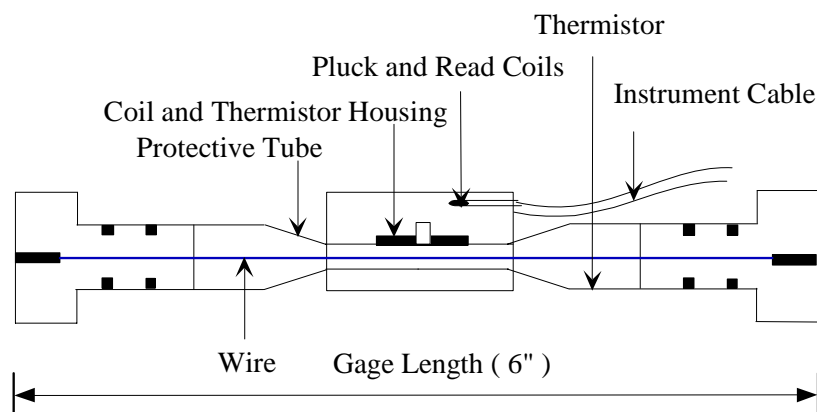
Table 3. Specifications for Vibrating Wire Strain Gages (VWSG)

Specifications	Model 4200
Standard Range	3000 micro strain (for each model)
Sensitivity (micro strain)	0.5 to 1.0
Accuracy	$\pm 0.1$ % F.S.
Nonlinearity	$< 0.5$ % F.S.
Temperature Range	$-20^{\circ}\text{C}$ to $+80^{\circ}\text{C}$ (for each model)
Active Gage Length	153 mm (6 in.)





(a) Picture of VWSG. Gage. (Source: Geokon Website, URL <http://www.geokon.com>)



(b) Sketch showing Working Mechanism of VWSG (Source: Geokon VWSG Instruction Manual).

Figure 11. Picture and working mechanism of VWSG.

### **Soil Strain Meter (Model 4430)**

Model 4430 Soil Strain Meter with flanged ends is designed to measure longitudinal deformation in dams and embankments. It can also be grouted or held in place by hydraulic anchors to measure deformations in boreholes (over the gage length). Specifications of this type of sensors are shown in Table 4. Figure 12(a) shows a photograph the VW deformation meter.

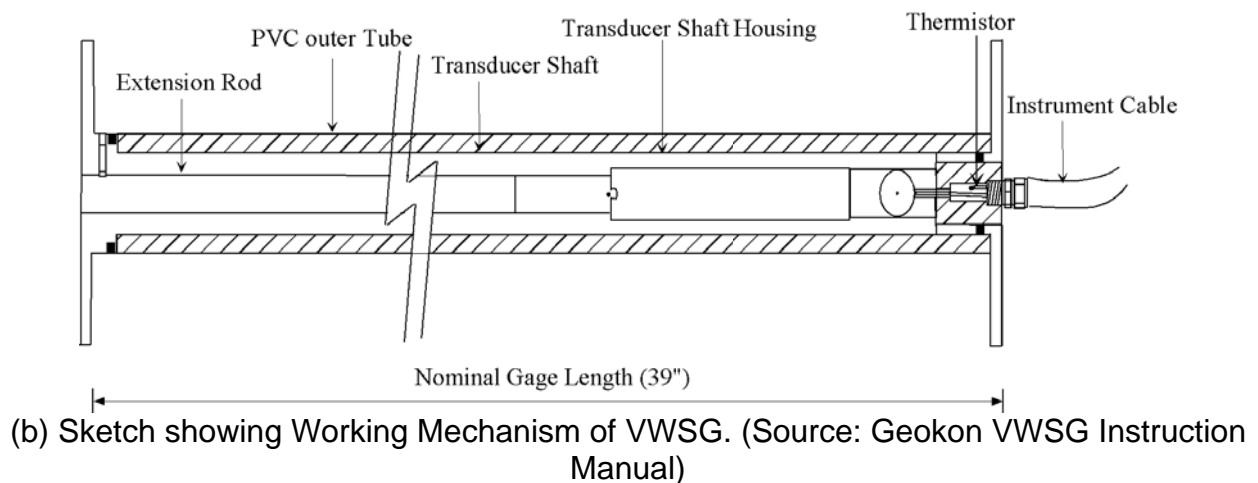
The gage sensor is attached to a flange at one end and, by a connecting rod of some length, to a flange at the other end. The sensor and the rod are covered by a plastic (PVC) tube which holds the end flanges apart at a predetermined distance (gage length) and insures that the rod is free to move. As the flanges move apart, the movement is conveyed by a connecting rod to the sensor and measured by the readout system. Figure 12(b) shows a sketch that explains the working mechanism for the VW Deformation Meter.

Table 4. Specifications for VW Deformation Meter. (Manual)

Specifications	Model 4430
Standard Range	25, 50, 100mm (1, 2, 4 in.)
Sensitivity (micro strain)	0.02% F.S.
Accuracy	$\pm 0.1$ % F.S.
Nonlinearity	$< 0.5$ % F.S.
Temperature Range	$-20^{\circ}\text{C}$ to $+80^{\circ}\text{C}$ (for each model)
Active Gage Length	Varies x 50 mm (2in.)



(a) Picture of VW Deformation Meter. (Source: Geokon Website, URL <http://www.geokon.com> e)



(b) Sketch showing Working Mechanism of VWSG. (Source: Geokon VWSG Instruction Manual)

Figure 12. Picture and working mechanism of VW Deformation Meter.

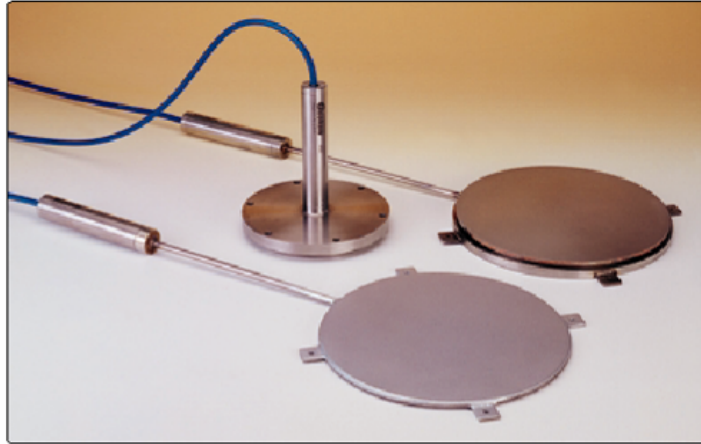
### **"Fat Back" Pressure Cell (Model 4810)**

The model 4810 "Fat-Back" Cell is intended to measure contact earth pressures on the surface of concrete or steel. The cell has an extra thick back plate to minimize any point loading effects. "Ears" on the cell assist in holding it to concrete forms or to retaining walls during installation. Specifications of this sensor are analyzed in Table 5. Figure 13(a) is a picture of the Pressure Cell.

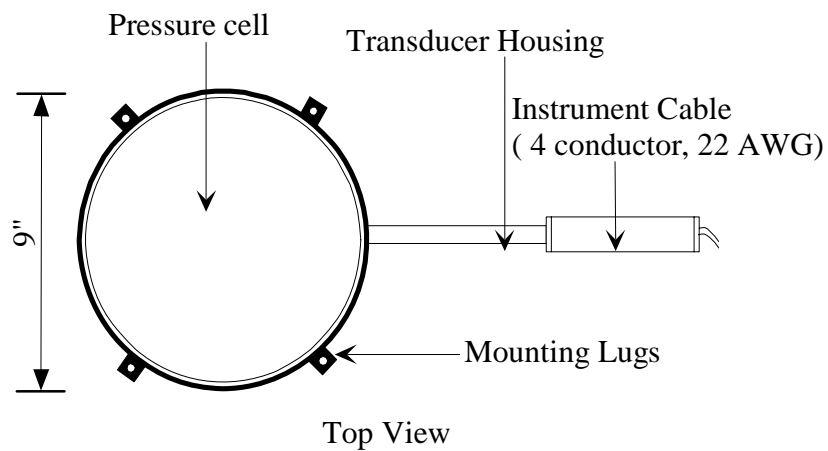
Earth pressure cells are constructed from two stainless steel plates welded together around their periphery and separated by a narrow gap filled with hydraulic fluid. External pressures squeeze the two plates together creating an equal pressure in the internal fluid. A length of stainless steel tubing connects the fluid filled cavity to a pressure transducer that converts the fluid pressure into an electrical signal transmitted by cable to the readout location. Figure 13(b) shows a sketch explaining the working mechanism of the Pressure Cell.

Table 5. Specifications of "Fat Back" Pressure Cell (Model 4810) (Manual)

Specifications	Model 4430
Standard Range	50, 100, 250, 500, 750 psi
Over range capacity	0.02% F.S.
Sensitivity	± 0.1 % F.S.
Accuracy	< 0.5 % F.S.
Height x Diameter	0.5 x 9 in.



(a) Picture of VW Deformation Meter. (Source: Geokon Website, URL <http://www.geokon.com>)



(b) Sketch showing Working Mechanism of Pressure Cell. (Source: Geokon Pressure Cell Instruction Manual)

Figure 13. Picture and working mechanism of Pressure Cell.

### **Settlement Sensor (Model 4650)**

The model 4650 is designed for remote measurement of the settlement of a point in or below fills, surcharges, embankments, etc. Specifications for this sensor are shown in . Figure 14(a) provides a picture of the Settlement Sensor.

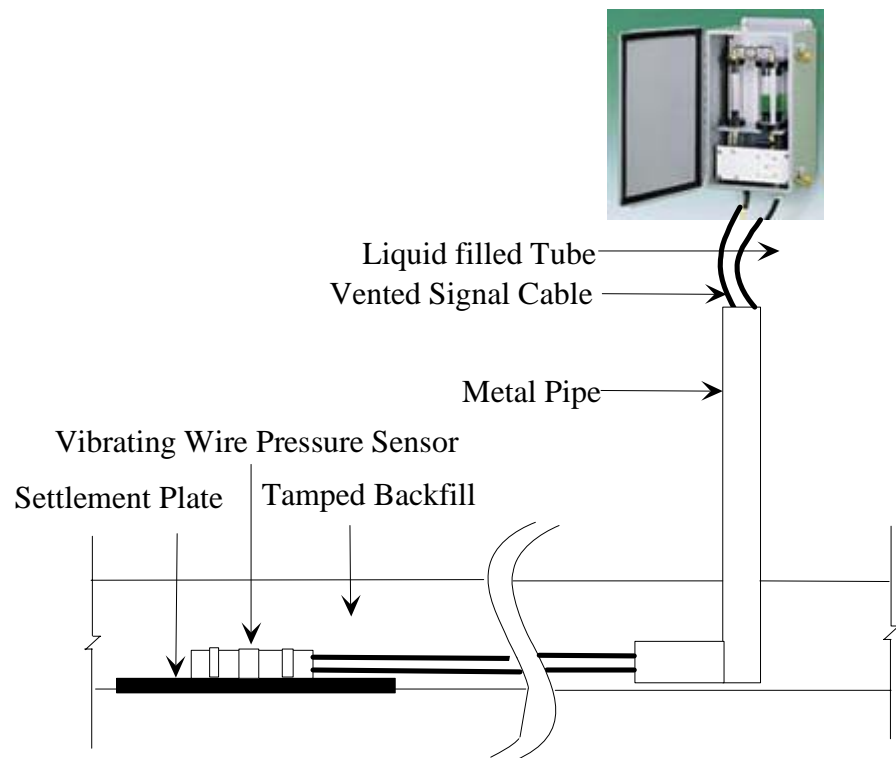
The Model 4650 Settlement System uses a Pressure Transducer attached to a settlement plate located in the settling ground. The sensor is connected, via two fluid-filled tubes, extending laterally, to a reservoir located on firm ground away from the area of anticipated movement. Fluid pressure within the tubes is sensed by the transducer, which provides a measure of elevation difference between the sensor and the reservoir. Figure 14(b) shows a sketch explaining working mechanism of Settlement Sensor.

Table 6. Specifications for Settlement Sensor, Model 4650.

Specifications	Model 4430
Standard Range	5, 15, 30, 60 psi
Sensitivity	0.025% F.S.
Accuracy	$\pm 0.25$ % F.S. to $\pm 1$ % F.S.
Height x Diameter	(Reservoir) 6 x 2in.
Height x Diameter	(Sensor) 7.5 x 1.375in.



(a) Picture of Settlement Sensor. (Source: Geokon Website, URL <http://www.geokon.com>)



(b) Sketch showing Working Mechanism of Settlement Sensor. (Source: Geokon Settlement Sensor Instruction Manual)

Figure 14. Picture and working mechanism of Settlement Sensor.

## **Installation of Sensors and WIM System**

### **VWSG**

The VWSGs are installed on the top and bottom layer of the steel reinforcement of the approach slab. Because the gages are 6 in. in length, they are first attached to two 18 in. supporting No. 3 epoxy coated reinforcing steels using zip lock ties. The two supporting steels are then tied to the approach steel reinforcement. The supporting steels are also used for protection of the gages from construction workers and equipments. Each gage is also carefully labeled to match the data logger channel to the gage. The cables are routed to the data logger inside metal conduits that protected the cable from the concrete pressure as well as construction equipment. All gages are tested for functionality with a portable readout box, GK-403. Figures Figure 15 and Figure 16 illustrate the VWSGs and installed VWSGs and their supporting steel, respectively.

### **VW Deformation Meter**

The VW deformation meter is used to measure the displacement between the concrete layer and the under layer soil, thus, portion of the meter is embedded in the concrete approach slab and the other portions in the soil layers. The VW deformation meter is embedded vertically 16 in. in the soil using Portland cement grout. Each meter is also carefully labeled to match the data logger channel to the meter. The cables are routed to the data logger inside metal conduits that protected the cable from the concrete pressure as well as construction equipment. All meters are tested for functionality with a portable readout box, GK-403. Figure 17a and 17b illustrate the drilled hole in the soil layer and the grouted meter, respectively.

### **Pressure Cell**

The Pressure Cell is installed at the same location of the deformation meter to check the contact between the approach slab and the under layer soil. It is simply placed on top of the soil layer at the desired location. Similarly, the cable is run and protected inside metal conduit to the data logger. All pressure cells are also tested using the GK-403 readout box. Figure 18 illustrates the pressure cell placement.

### **Settlement Sensor**

The settlement sensor is installed in the center between the two lanes on north and south approach slabs. The settlement is intended to measure the settlement as is supposed to be installed underneath the surcharge. However, since the instrumentation of the approach slab is later implemented, the sensor was installed in a small 15 in. deep trench was constructed with an inclination so that the sensor will be below the liquid reservoir located in the data logger box. Figure 19 illustrates the settlement

sensor installed inside the trench. The trench is covered with soil and compacted prior to the casting of the approach slabs.



Figure 15. VWSG Connected to Wires Ready for Delivery and Installation on Site.

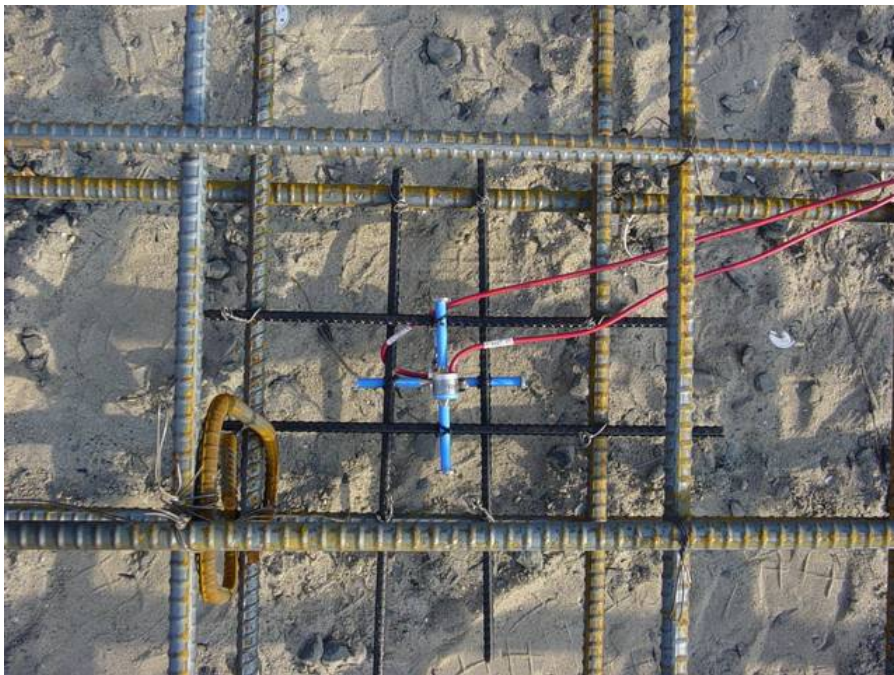


Figure 16. VWSG installed Longitudinally and Transversely at Site.





(a)



(b)

Figure 17. (a) Embedded and (b) grouted VW Deformation Meter.

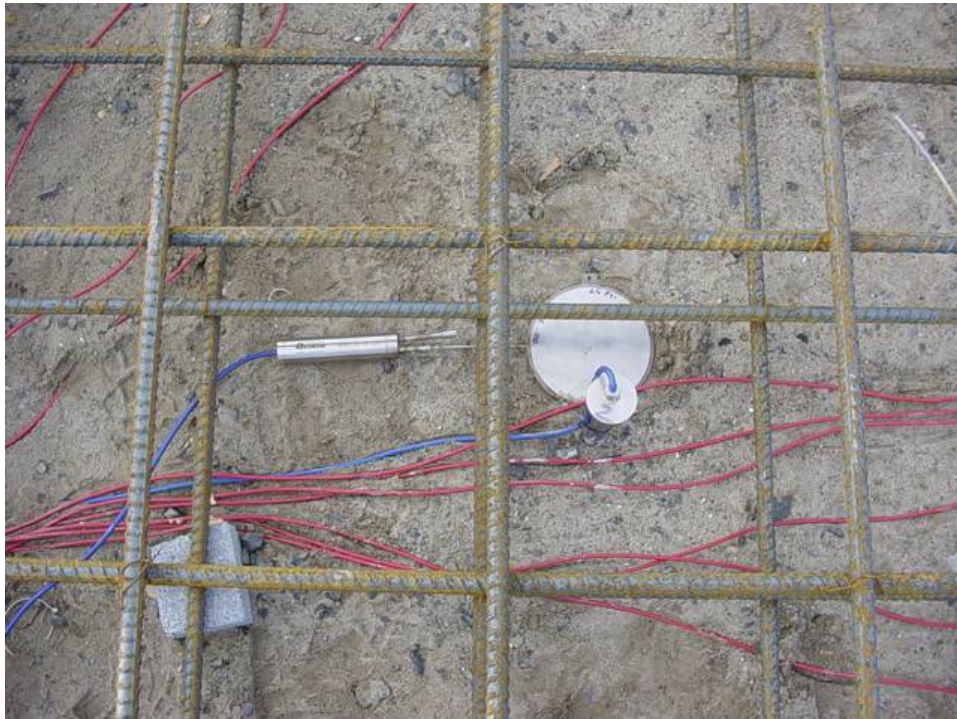


Figure 18. Pressure Cell installed underneath Approach Slab near the VW Deformation Meter.

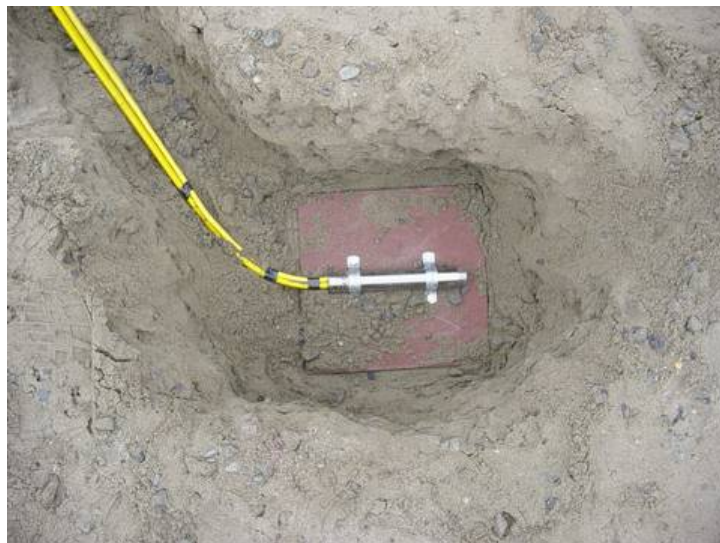


Figure 19. Settlement Sensor installed in Soil strata underneath Approach Slab.



## **Data Logger**

Campbell Scientific CR10X data logger is used to collect all the data from all the sensors. Multiplexers are used to expand the data logger channel count to a maximum of 96 channels. The data logger is programmed to take readings every 5 minutes. The maximum and minimum readings are also captured hourly. The data logger also has two modes of capturing the data: (1) every 5 minutes interval or (2) every hour interval. The second mode is designed to conserve the limited memory of the data logger. In addition, the data logger is connected to a solar power that charged the data logger battery. Figure 20 and 21 illustrate the data logger and wiring connection, respectively.



Figure 20. Data logger box and Solar Panel installed on wing wall.



Figure 21. Downloading Data from Data-Logger Using Portable Computer.

## Weigh-In-Motion (WIM) System Installation

WIM System is used to measure the weight, speed, and type of trucks passing on the bridge. WIM plates are installed on SA-LN-3 and SA-LN-4 approach slabs. As the wheel of a truck hits these plates, time, type of truck (i.e., 3axle, 4axle, 5axle etc.), total weight of truck (with weight of each individual axles), and speed of the truck are recorded and saved. Figure 22 illustrates the location of WIM plates installed on SA-LN-3 and SA-LN-4. Conduits are laid for running the cables of the WIM system before the reinforcement cage is placed, (Figure 23). After placing the reinforcement, the rebars are cut at locations of WIM plates and are placed 7" from top of the slab. 22 days after the first pouring and 15 days after the second pour, the concrete is cut at the WIM locations, and WIM Plates are installed, as shown in Figure 24.

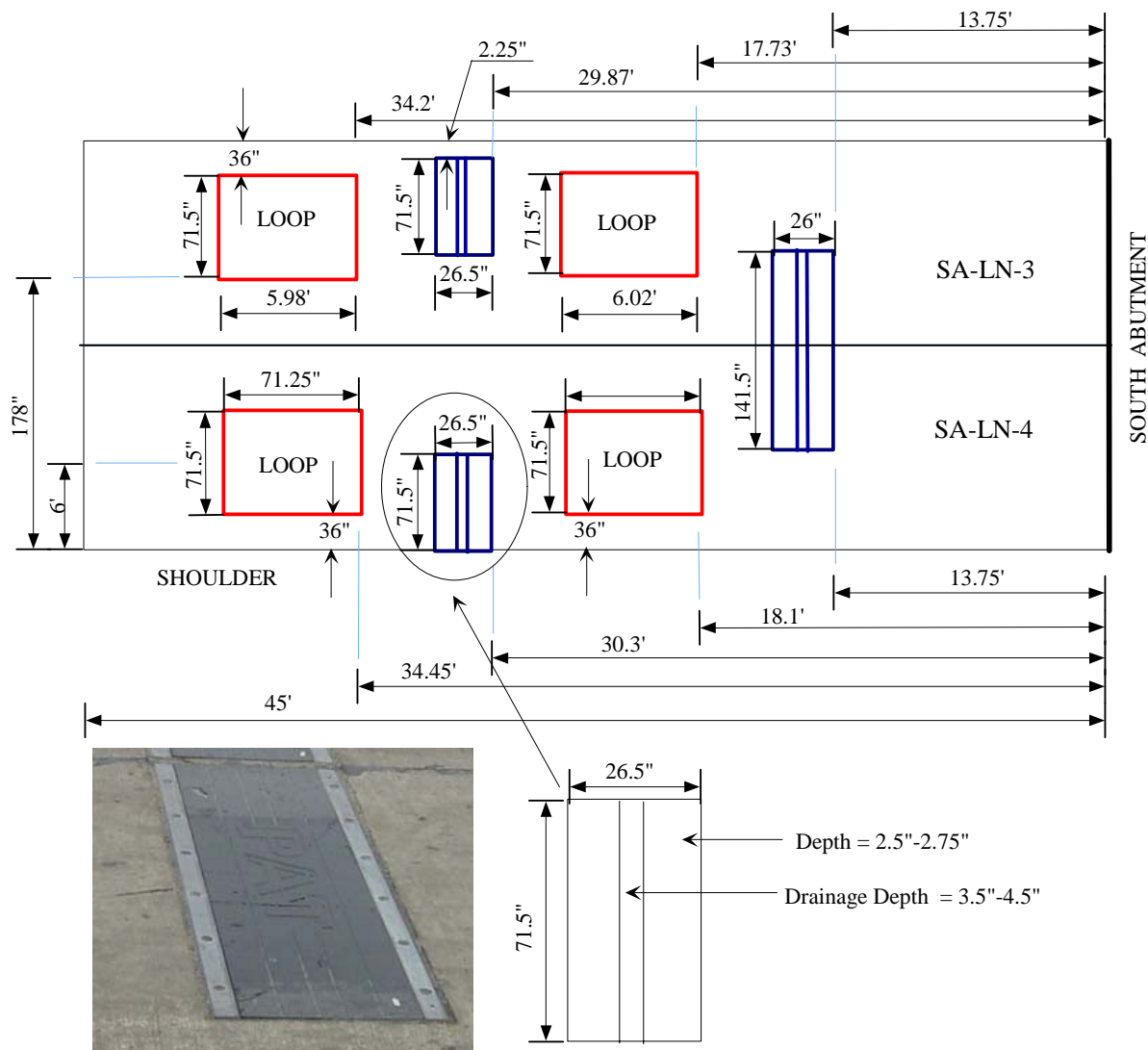


Figure 22. Bending Plate Fixed WIM System Installed on SA-LN-3 and SA-LN-4.



Figure 23. Conduits laid for WIM System Installation at South Abutment.



Figure 24. Bending Plate WIM System with Loop Detectors installed at the South Abutment.

## Concreting Sequence

Diagram illustrating the plan view of the bridge deck and approach slabs, showing lane configurations and construction status.

**Bridge Deck Dimensions and Layout:**

- Overall Width:** 55'
- Approach Slabs:** 45' (South) and 35' (North)
- Lane Configurations:**
  - Lane 1:** Open to Traffic (Width: 17')
  - Lane 2:** Open to Traffic (Width: 17')
  - Lane 3:** Under construction (Width: 12')
  - Lane 4:** Under construction (Width: 12')
- Shoulders:** Located on both sides of the bridge deck.
- Construction Status:** Lanes 1 and 2 are open to traffic; Lanes 3 and 4 are under construction.
- Approach Slabs:** Labeled "POUR-1" and "POUR-2" on both sides.
- Abutments:** SOUTH ABUTMENT and NORTH ABUTMENT.
- Bridge Structure:** BRIDGE.

POUR-2 : 1st November'2002

Figure 25. Concrete pouring sequence of approach slabs on the Doremus Avenue Bridge.

1. Figure 26 depicts the concreting of approach slabs.
2. Rebar are inserted at slab edges immediately after concreting to ensure continuity of that slab with the adjacent one.
3. A curing compound is applied to approach slabs immediately after concreting.
4. The approach slab is then covered with burlap, about one hour the after curing compound was applied.



Figure 26. Concreting of Approach Slab for Concrete Pour No. 1.

### **Sampling**

1. Concrete samples (cylinders of size 4" by 6") are taken at the same time of concreting and with same concrete mix used for approach slabs in each Lane.
2. Curing compound is applied to top of concrete cylinders immediately after filling them with concrete.
3. Concrete cylinders are covered with Burlap half an hour after taking samples as shown in Figure 27.





Figure 27. Concrete Cylinders Cured on Site using Burlap.

### **Testing**

1. Concrete samples are kept on the site itself, so that they would remain in the same environmental conditions as the approach slabs.
2. Cylinders are brought from the site at different intervals of days and tested for compressive strength and elastic modulus.
3. Three cylinders from each slab are picked up at 5, 7, 15, and 31 days and are tested for compressive strength value. The average of the three values is considered as the compressive strength of that slab. Figure 28. shows the results of the Compressive strengths of the approach slabs of the south side lane 4 and north side lane 3.
4. It is observed that SA-LN-3 has a compressive strength of 5670 psi, and NA-LN-4 has a compressive strength of 5570 psi.
5. Three cylinders from each slab are picked up at 5, 7, 15, and 31 days and are tested to find the elastic modulus of the concrete used in slabs.
- 6.
7. Figure 29 shows set up for measuring the elastic modulus. Cylinders are loaded up to 40% of their compressive strength, and readings for change in lengths are taken at certain intervals of loads to get the values of strains at those particular loads.
8. Stresses are found for each load.
9. Elastic Modulus can be expressed as the ratio of strain to stress.
10. Figure 30 shows a comparison of results between the elastic modulus for SA-LN-3 and NA-LN-4.



11. It is found that at 43 days, the modulus of elasticity for SA-LN-3 and NA-LN-4 is  $4.188 \text{ E}+6 \text{ psi}$  and  $4.114 \text{ E}+6 \text{ psi}$ , respectively.

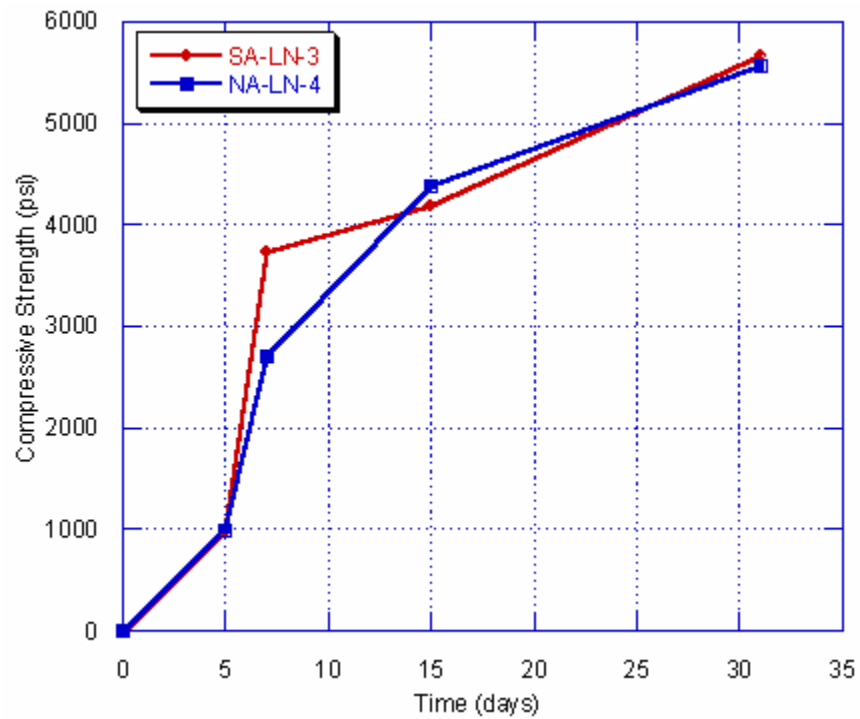


Figure 28. Comparison of Compressive Strengths for Concrete Pour-2.



Figure 29. Experimental Setup for testing the Elastic Modulus of Concrete

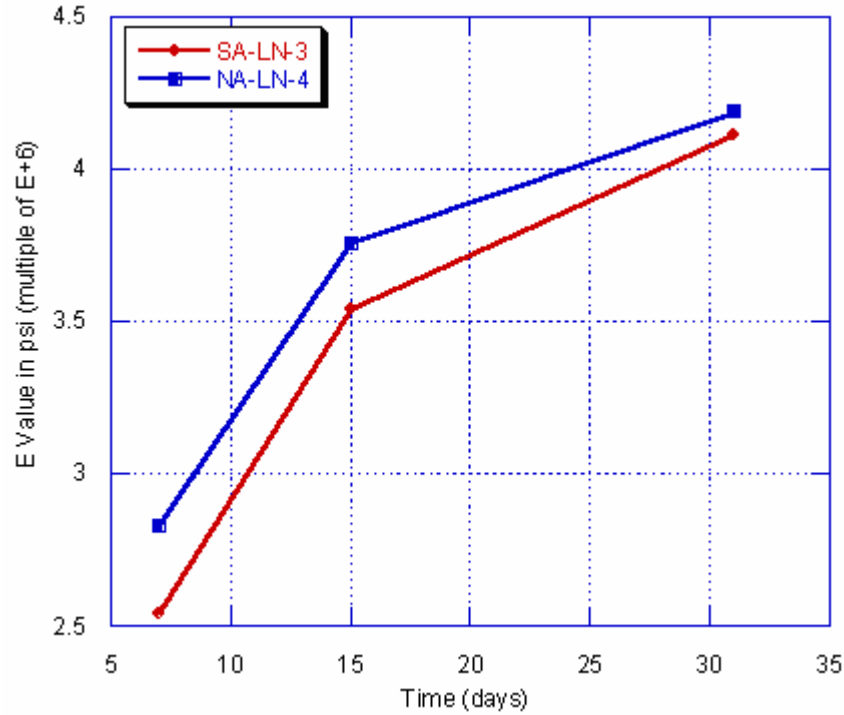


Figure 30. Comparison of Elastic Modulus for two slabs of Concrete Pour No. 2.

## STATIC TESTING

### Test Truck Information and Testing Procedure

Static tests are performed for three slabs (SA-LN-3, SA-LN-4, and NA-LN-4) at various truck positions. A truck is placed at different locations of approach slabs, traveling in both the directions.

Figure 31a shows the truck at the entrance of the approach slab,

Figure 31b shows the truck leaving the approach slabs,

Figure 31c shows the truck in the middle of the approach slabs, and

Figure 31d shows the truck with the one-side wheels of the axles on approach slab.

Details of the truck used for testing are given in Table 7.



(a)



(b)



(c)



(d)

Figure 31. Various Truck Positions for Static Load Testing of new Approach Slabs.

Table 7. Information of Truck, used for Approach Slab Testing.

Total Number of Axles	3
Weight of Steer Axle in lbs	16100
Weight of Drive Axle in lbs	36520
Weight of Trailer Axle in lbs	24980
Gross Weight of Truck in lbs	77600
Distance between Steer Axle and Drive Axle	14' 6"
Distance between Drive Axle and Trailer Axle	6' 9"
c/c distance between wheels of the Axle	6'
Overall width of the Truck	8'

Strain and temperature readings of all sensors are taken just before placing the test truck on the approach slabs. These readings are considered as zero reference readings, which are subtracted from the readings for various truck positions to get the change in the strain in vibrating wire strain gages.

Finite Element Models are used to predict change in strains in vibrating wire strain gages. The same truck used for testing, is also used in the FE Model and the results are compared with field results. Table 8 (a, b, c, and d), Table 9(a, b, c, and d) and Table 10 (a, b, c, and d) show a comparison of the finite element model results with the field testing results for NA-LN-3, SA-LN-3 and SA-LN-4 respectively. For different truck configurations, which are very close to the position of the truck wheels for different positions of truck, it is found that results from the FEM and the field-testing are very close.

Table 8. Comparison of the finite element results and the field results for NA-LN-3.

(a). Truck heading northbound and both wheels of axles on approach slab.

Test	Truck Position	Sensor No.	Sensor Location	FEM	FIELD	Difference
	(from abutment)		(from abutment)	( $\mu$ strain)	( $\mu$ strain)	( $\mu$ strain)
1	F (3.5', 3') (3.5', 9')	17	(5', 6')	5	5	0
2	F (6.5', 3') (6.5', 9')	17	(5', 6')	7	6	1
3	F (6.5', 3') (6.5', 9')	24	(17.5', 9')	7	5	2
		25(Trans)	(17.5', 9')	3	3	0
		26	(17.5', 6')	4	3	1
		27	(17.5', 3')	5	4	1
		28 (Trans)	(17.5', 3')	7	4	3
	M (3.5', 3') (3.5', 9')	17	(5', 6')	1	1	0
5	F (31.5', 3') (31.5', 9')	30	(35', 9')	3	1	2
		31	(35', 6')	3	2	1
		32	(35', 3')	2	1	1
	M (6.5', 3') (6.5', 9')	24	(17.5', 9')	3	2	1
		25(Trans)	(17.5', 9')	3	4	-1
		26	(17.5', 6')	4	1	3
		27	(17.5', 3')	3	1	2
		28 (Trans)	(17.5', 3')	7	4	3
	R (11.25', 3') (11.25', 9')	19	(11.25', 9')	12	13	-1
		20	(11.25', 6')	14	14	0
		21 (Trans)	(11.25', 6')	4	4	0
6	M (31.5', 3') (31.5', 9')	30	(35', 9')	6	5	1
		31	(35', 6')	7	7	0
		32	(35', 3')	6	5	1
	R (3.5', 3') (3.5', 9')	29	(24', 6')	6	3	3
7	R (33.5', 3') (33.5', 9')	30	(35', 9')	4	2	2
		31	(35', 6')	1	2	-1
		32	(35', 3')	3	2	1

Table 8 (b). Truck heading northbound and one wheel of an axle on approach slab.

Test	Truck Position (from abutment)	Sensor No.	Sensor Location (from abutment)	FEM ( $\mu$ strain)	FIELD ( $\mu$ strain)	Difference ( $\mu$ strain)
8	F(33.5', 92")	30	(35', 9')	1	1	0
		31	(35', 6')	6	2	4
		32	(35', 3')	4	1	3
	M (17', 92")	24	(17.5', 9')	2	4	-2
		25(Trans)	(17.5', 9')	9	2	7
		26	(17.5', 6')	7	2	5
		27	(17.5', 3')	4	3	1
		28 (Trans)	(17.5', 3')	0	1	-1
	R (10.25', 92")	19	(11.25', 9')	6	13	-7
		20	(11.25', 6')	6	11	-5
		21 (Trans)	(11.25', 6')	4	2	2
9	M (31.5', 92")	30	(35', 9')	5	5	0
		31	(35', 6')	5	5	0
		32	(35', 3')	3	3	0
	R (3.5', 3') (3.5', 9')	29	(24', 6')	5	3	2
10	F (33.5', 92")	30	(35', 9')	2	2	0
		31	(35', 6')	6	0	6
		32	(35', 3')	6	0	6

Table 8 (c). Truck heading southbound and both wheels of axles on approach slab.

Test	Truck Position	Sensor No.	Sensor Location	FEM	FIELD	Difference
	(from abutment)		(from abutment)	( $\mu$ strain)	( $\mu$ strain)	( $\mu$ strain)
16	R (31.5', 3') (31.5', 9')	30	(35', 9')	4	2	2
		31	(35', 6')	5	4	1
		32	(35', 3')	4	3	1
19	F (6.5', 3') (6.5', 9')	17	(5', 6')	2	6	-4
	M (21', 3') (21', 9')	24	(17.5', 9')	2	2	0
		25(Trans)	(17.5', 9')	3	3	0
		26	(17.5', 6')	3	2	1
		27	(17.5', 3')	3	1	2
		28 (Trans)	(17.5', 3')	3	3	0
	R (28', 3') (28', 9')	29	(24', 6')	13	9	4
		30	(35', 9')	7	3	4
		31	(35', 6')	8	5	3
		32	(35', 3')	7	5	2
20	M (6.5', 3') (6.5', 9')	17	(5', 9')	4	10	-6
	R (13', 3') (13', 9')	18 (Top)	(11.25', 9')	6	16	-10
		19	(11.25', 9')	6	18	-12
		20	(11.25', 6')	5	19	-14
		21 (Trans)	(11.25', 6')	1	6	-5
		22 (Top)	(11.25', 3')	6	15	-9
		23	(11.25', 3')	6	18	-12
21	R (3.5', 3') (3.5', 9')	17	(5', 6')	5	4	1

Table 8 (d). Truck heading southbound and one wheel of an axle on approach slab.

Test	Truck Position	Sensor No.	Sensor Location	FEM	FIELD	Difference
	(from abutment)		(from abutment)	( $\mu$ strain)	( $\mu$ strain)	( $\mu$ strain)
22	F (31.5', 3') (31.5', 9')	30	(35', 9')	3	2	1
		31	(35', 6')	3	4	-1
		32	(35', 3')	1	2	-1
24	M (3.5', 95")	17	(5', 6')	3	1	2
	F (17.5', 3') (17.5', 9')	24	(17.5', 9')	9	7	2
		25(Trans)	(17.5', 9')	3	4	-1
		26	(17.5', 6')	7	5	2
		27	(17.5', 3')	3	4	-1
		28 (Trans)	(17.5', 3')	1	2	-1
25	R (33.75', 95")	30	(35', 9')	4	6	-2
		31	(35', 6')	3	6	-3
		32	(35', 3')	2	4	-2
	M (27', 95")	29	(24', 6')	2	3	-1
	F (12.5', 95")	18 (Top)	(11.25', 9')	9	9	0
		19	(11.25', 9')	7	8	-1
		20	(11.25', 6')	9	9	0
		21 (Trans)	(11.25', 6')	5	3	2
		22 (Top)	(11.25', 3')	5	9	-4
		23	(11.25', 3')	5	8	-3



Table 9. Comparison of Results for the finite element and the field tests for SA-LN-3.

(a). Truck heading southbound and one wheel of an axle on approach slab.

Test	Truck Position	Sensor no.	Sensor Location	FEM	FIELD	Difference
	(from abutment)		(from abutment)	( $\mu$ strain)	( $\mu$ strain)	( $\mu$ strain)
14	F (40', 3')	32	(40', 6')	3	1	2
15	F (19', 3')	24	(22', 3')	2	12	-10
		25 (Trans)	(22', 3')	3	5	-2
	M (34', 3')	30 (Top)	(32', 3')	3	7	-4
		31	(32', 3')	3	16	-13
	R (41', 3')	32	(40', 6')	4	5	-1
16	F (5', 3')	18	(5', 6')	2	2	0
		19	(5', 3')	2	1	1
	M (20', 3')	24	(22', 3')	8	14	-6
		25 (Trans)	(22', 3')	7	6	1
	R (27', 3')	-	-	-	-	-
17	M (5', 3')	19	(5', 3')	8	3	5
		18	(5', 6')	7	3	4
	R (12', 3')	32	(40', 6')	7	11	-4
18	F (3', 3')	19	(5', 3')	7	0	7
		18	(5', 6')	6	0	6
25	F (8', 100")	17	(5', 9')	0	2	-2
		18	(5', 6')	0	1	-1
	M (22', 100")	21	(22', 9')	15	16	-1
		22 (Trans)	(22', 9')		6	-6
	R (29', 100")	-	-	-	-	-
26	R (3', 100")	17	(5', 9')	0	0	0
		18	(5', 6')	0	1	-1

Table 9 (b). Truck heading southbound and both wheels of axles on approach slab.

Test	Truck Position	Sensor no.	Sensor Location	FEM	FIELD	Difference
	(from abutment)		(from abutment)	( $\mu$ strain)	( $\mu$ strain)	( $\mu$ strain)
19	R (40', 3') (40', 9')	32	(40', 6')	4	3	1
21	F (19', 3') (19', 9')	21	(22', 9')	1	16	-15
		22 (Trans)	(22', 9')	1	5	-4
		23	(22', 6')	0	16	-16
		24	(22', 3')	1	14	-13
		25 (Trans)	(22', 3')	3	5	-2
	M (34', 3') (34', 9')	26 (Top)	(32', 9')	4	2	2
		27	(32', 9')	8	12	-4
		28	(32', 6')	10	14	-4
		29 (Trans)	(32', 6')	10	2	8
		30 (Top)	(32', 3')	8	5	3
		31	(32', 3')	4	14	-10
22	F (40', 3') (40', 9')	17	(5', 9')	6	4	2
		18	(5', 6')	3	2	1
		19	(5', 3')	2	3	-1
	M (20', 3') (20', 9')	21	(22', 9')	14	22	-8
		22 (Trans)	(22', 9')	7	1	6
		23	(22', 6')	17	23	-6
		24	(22', 3')	14	21	-7
		25 (Trans)	(22', 3')	6	3	3
	R (27', 3') (27', 9')	-	-	-	-	-
23	M (5', 3') (5', 9')	17	(5', 9')	16	5	11
		18	(5', 6')	19	5	14
		19	(5', 3')	16	5	11
	R (12', 3') (12', 9')	20	(13', 6')	9	12	-3
24	R (3', 3') (3', 9')	17	(5', 9')	11	0	11
		18	(5', 6')	12	0	12
		19	(5', 3')	11	0	11

Table 9 (c). Truck heading northbound and one wheel of an axle on approach slab.

Test	Truck Position	Sensor no.	Sensor Location	FEM	FIELD	Difference
	(from abutment)		(from abutment)	( $\mu$ strain)	( $\mu$ strain)	( $\mu$ strain)
40	F (5', 3')	19	(5', 3')	4	3	1
		18	(5', 6')	3	3	0
41	F (22', 44")	24	(22', 3')	5	24	-19
		25 (Trans)	(22', 3')	4	9	-5
	M (7', 44")	19	(5', 3')	9	2	7
		18	(5', 6')	9	2	7
	R (9", 44")	-	-	-	-	-
42	F (40', 44")	32	(40', 6')	1	6	-5
	M (25', 44")	24	(22', 3')	6	25	-19
		25 (Trans)	(22', 3')	4	9	-5
	R (18', 44")	-	-	-	-	-
43	M (40', 44")	32	(40', 6')	8	7	1
		30 (Top)	(32', 3')	4	17	-13
		31	(32', 3')	4	34	-30
		28	(32', 6')	4	26	-22
		29 (Trans)	(32', 6')	3	5	-2
44	R (33', 44")	32	(40', 6')	5	5	0

Table 9 (d). Truck heading northbound and both wheels of axles on approach slab.

Test	Truck Position	Sensor no.	Sensor Location	FEM	FIELD	Difference
	(from abutment)		(from abutment)	( $\mu$ strain)	( $\mu$ strain)	( $\mu$ strain)
45	F (5', 3') (5', 9')	17	(5', 9')	8	6	2
		18	(5',6')	8	5	3
		19	(5',3')	8	5	3
46	F (22', 3') (22', 9')	21	(22', 9')	6	29	-23
		22 (Trans)	(22', 9')	3	6	-3
		23	(22', 6')	4	29	-25
		24	(22', 3')		29	-29
		25 (Trans)	(22', 3')	4	6	-2
	M (7', 3') (7', 9')	17	(5', 9')	3	2	1
		18	(5',6')	14	2	12
		19	(5',3')	12	1	11
	R (9", 3') (9", 9')	-	-	-	-	-
47	F (40', 3') (40', 9')	32	(40',6')	6	8	-2
	M (22', 3') (22', 9')	21	(22', 9')	1	31	-30
		22 (Trans)	(22', 9')	0	4	-4
		23	(22', 6')	12	32	-20
		24	(22', 3')	1	29	-28
		25 (Trans)	(22', 3')	0	6	-6
	R (9", 3') (9", 9')	-	-	-	-	-
48	M (40', 3') (40', 9')	32	(40',6')	16	10	6
	R (33', 3') (33', 9')	26 (Top)	(32', 9')	7	9	-2
		27	(32', 9')	7	24	-17
		28	(32', 6')	8	27	-19
		29 (Trans)	(32', 6')	2	2	0
		30 (Top)	(32', 3')	7	16	-9
		31	(32', 3')	7	34	-27
49	R (42', 3') (42', 9')	32	(40',6')	2	4	-2

Table 10. Comparison of the finite element results and the field results for SA-LN-4.  
(a). Truck heading northbound and both wheels of axles on approach slab.

Test	Truck Position	Sensor no.	Sensor Location	FEM	FIELD	Difference
	(from abutment)		(from abutment)	( $\mu$ strain)	( $\mu$ strain)	( $\mu$ strain)
1	F (40', 3')	14	(40', 9')	5	3	2
		15	(40', 6')	6	1	5
		16	(40', 3')	5	2	3
3	F (22', 3') (22', 9')	8	(22', 9')	7	10	-3
		9 (Trans)	(22', 9')	5	5	0
		10	(22', 6')	4	9	-5
		11	(22', 3')	7	12	-5
		12 (Trans)	(22', 3')	5	1	4
	M (36', 3') (36', 9')	-	-	-	-	-
	R (36', 3') (36', 9')	1	(5', 6')	1	0	1
4	F (19', 3') (19', 9')	-	-	-	-	-
	M (34', 3') (34', 9')	13	(32', 6')	8	5	3
	R (44', 3') (44', 9')	1	(5', 6')	1	0	1
5	F (8', 3') (8', 9')	1	(5', 6')	1	1	0
	F (22', 3') (22', 9')	8	(22', 9')	10	9	1
		9 (Trans)	(22', 9')	7	4	3
		10	(22', 6')	13	9	4
		11	(22', 3')	10	11	-1
		12 (Trans)	(22', 3')	1	1	0
	R (44', 3') (44', 9')	1	(32', 6')	9	14	-5
6	F (5', 3') (5', 9)	1	(5', 6')	8	3	5
	M (20', 3') (20', 9')	8	(22', 9')	4	15	-11
		9 (Trans)	(22', 9')	4	5	-1
		10	(22', 6')	4	16	-12
		11	(22', 3')	4	19	-15
		12 (Trans)	(22', 3')	2	2	0
	R (44', 3') (44', 9')	13	(32', 6')	6	8	-2

Table 10 (a). (Cont'd)

Test	Truck Position	Sensor no.	Sensor Location	FEM	FIELD	Difference
	(from abutment)		(from abutment)	( $\mu$ strain)	( $\mu$ strain)	( $\mu$ strain)
7	M (5', 3')(5', 9')	1	(5', 6')	19	3	16
	M (12', 3') (12', 9')	2 (Top)	(13', 9')	17	6	11
		3	(13', 9')	17	14	3
		4	(13', 6')	14	16	-2
		5	(13', 6')	2	3	-1
		6 (Top)	(13', 3')	8	5	3
		7	(22', 3')	8	0	8
8	R (3', 3') (3', 9')	1	(5', 6')	13	1	12

Table 10 (b). Truck heading northbound and one wheel of an axle on approach slab.

Test	Truck Position	Sensor no.	Sensor Location	FEM	FIELD	Difference
	(from abutment)		(from abutment)	( $\mu$ strain)	( $\mu$ strain)	( $\mu$ strain)
9	R (40', 3')	16	(40', 3')	4	3	1
		15	(40', 6')			
12	M (5', 3')	1	(5', 6')	15	5	10
	M (12', 3')	6 (Top)	(13', 3')	8	2	6
		7	(13', 3')	8	0	8
14	F (40', 9')	14	(40', 9')	2	2	0
		15	(40', 6')	4	1	3
15	F (19', 9')	8	(5', 9')	2	12	-10
		9 (Trans)	(5', 6')	2	1	1
	M (34', 9')	13	(13', 6')	8	11	-3
	R (41', 9')	14	(5', 6')	7	4	3
17	M (5', 9')	1	(5', 6')	14	4	10
	F (12', 9')	2 (Top)	(13', 9')	18	5	13
		3	(13', 9')	18	12	6

Table 10 (c). Truck heading southbound and both wheels of axles on approach slab.

Test	Truck Position	Sensor no.	Sensor Location	FEM	FIELD	Difference
	(from abutment)		(from abutment)	( $\mu$ strain)	( $\mu$ strain)	( $\mu$ strain)
35	F (5', 30") (5', 102")	19	(5', 3')	7	6	1
36	F(20', 30")(22', 102")	8	(22', 9')	7	29	-22
		9 (Trans)	(22', 9')	6	8	-2
		10	(22', 6')	4	26	-22
		11	(22', 3')	7	31	-24
		12 (Trans)	(22', 3')	5	2	3
	M(37', 30")(37', 102")	1	(5', 6')	1	3	
	R (9', 30") (9', 102")	-	-	-	-	-
37	F(40', 30")(40', 102")	14	(40', 9')	4	9	-5
		15	(40', 6')	3	3	0
		16	(40', 3')	4	6	-2
	F(25', 30")(25', 102")	-	-	-	-	-
	F(18', 30")(18', 102")	-	-	-	-	-
38	M(40', 44")(40', 102")	14	(40', 9')	14	12	2
		15	(40', 6')	16	7	9
		16	(40', 3')	17	8	9
	F(18', 30")(18', 102")	13	(32', 6')	9	23	-14
39	R(42', 30")(42', 102")	14	(40', 9')	0	4	-4
		15	(40', 6')	0	0	0
		16	(40', 3')	1	2	-1

Table 10 (d). Truck heading southbound and one wheel of an axle on approach slab.

Test	Truck Position (From Abutment)	Sensor no.	Sensor Location (from abutment)	FEM ( $\mu$ strain)	FIELD ( $\mu$ strain)	Difference ( $\mu$ strain)
40	F (5', 100")	1	(5', 6')	4	5	-1
41	F (22', 100")	8	(22', 9')	2	27	-25
		9 (Trans)	(22', 9')	1	4	-3
	M (37', 100")	13	(33', 6')	2	23	-21
	R (9", 100")	-	-	-	-	-
42	F (22', 100")	14	(40', 9')	1	6	-5
		15	(40', 6')	1	4	-3
	M (25', 100")	8	(22', 9')	6	29	-23
		9 (Trans)	(22', 9')	3	4	-1
	R (18', 100")	-	-	-	-	-
43	M (40', 100")	14	(40', 9')	4	8	-4
		15	(40', 6')	3	6	-3
	R (33', 100")	13	(33', 6')	4	24	-20
51	M (40', 100")	16	(22', 3')	4	6	-2
		15	(22', 3')	3	6	-3
	F (33', 100")	13	(13', 3')	4	28	-24

### Results from Available Sensor Data

Readings of sensors from Pour-1 (i.e., SA-LN-4, and NA-LN-3) are taken manually for the initial 21 days, and after that, the sensors are connected to a data logger. Readings of sensors from Pour 2, SA-LN-3 are taken manually for the first 14 days, and then the sensors are connected to a data logger. Sensors of Pour-2, NA-LN-4 are connected to a temporary data logger initially and then they are connected to permanent data logger.

Readings from each sensor are multiplied by their calibration factor, and, a temperature correction factor is also applied to get the final value in true strains of each sensor. True strains are found for each sensor, and they are plotted against time. Shrinkage behavior of concrete is studied from the available strain data.

Shrinkage of concrete is the time dependent strain measured for a concrete specimen or structure in its unloaded condition. If concrete structures are free to shrink, without restraint, shrinkage of concrete would not be a major concern to structural engineers. However, this is not the case. Contraction of concrete is always restraint by its supports or by adjacent structures. Each of these forms of restraint involves the imposition of a gradually increasing tensile force on the concrete, which may lead to time-dependent



cracking, increases in deflection, and a widening of existing cracks. Restraint to shrinkage is probably the most common cause of unsightly cracking in concrete structures. Figure 32(a) illustrates a free shrinkage condition. Free shrinkage causes volume change but does not create stresses. Figure 32(b) shows a restrained shrinkage condition. Restrained shrinkage causes stresses, which may lead to cracking of a concrete structure. Approach slabs were inspected for shrinkage cracks and no crack was found on any of the slab.

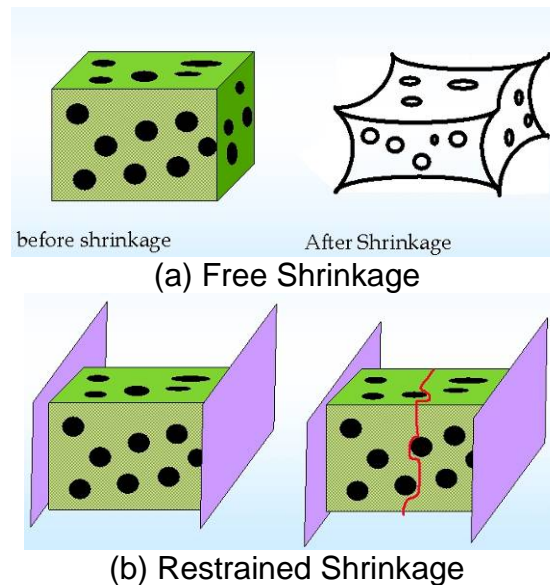


Figure 32. Shrinkage in Concrete Structures.

### VWSG Results from NA-LN-3.

1. Concreting of NA-LN-3 is executed in the first pour.
2. Figure 33 shows plots of shrinkage along the edge of the slab, which is towards NA-LN-4. A sensor in middle is showing higher strain than other sensors.
3. Figure 34 shows plots of shrinkage along the middle edge of the slab. Most of the sensors are showing the same value of strains. This makes sense, because all are confined by concrete from both the sides.
4. Figure 35 shows plots of shrinkage for all transverse sensors. Transverse sensors are showing less shrinkage than longitudinal ones. This is logical; sense because the length is smaller in that direction.

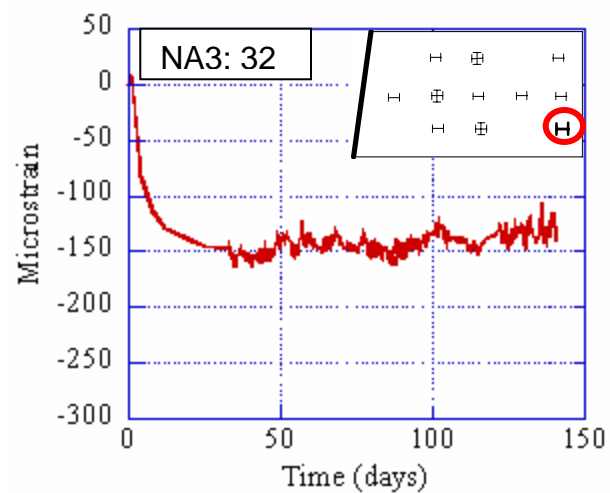
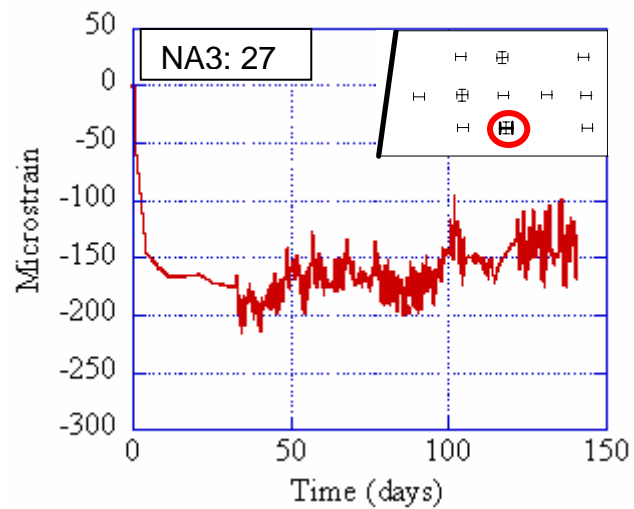
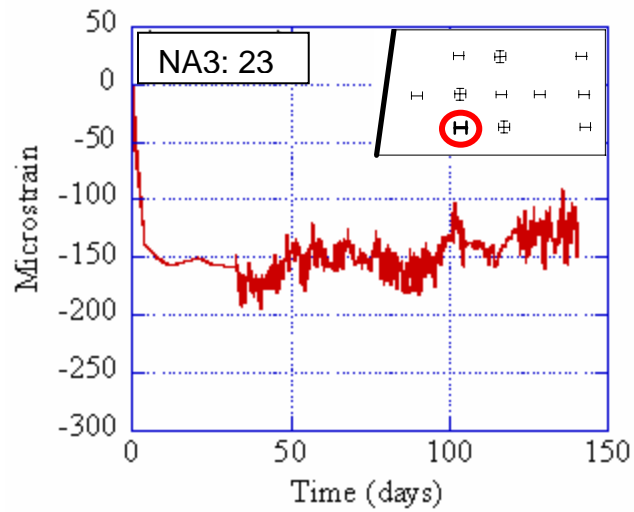


Figure 33. Shrinkage plots for sensors along edge towards Lane-4. (NA-LN-3) (From-10/24/02-03/14/03)

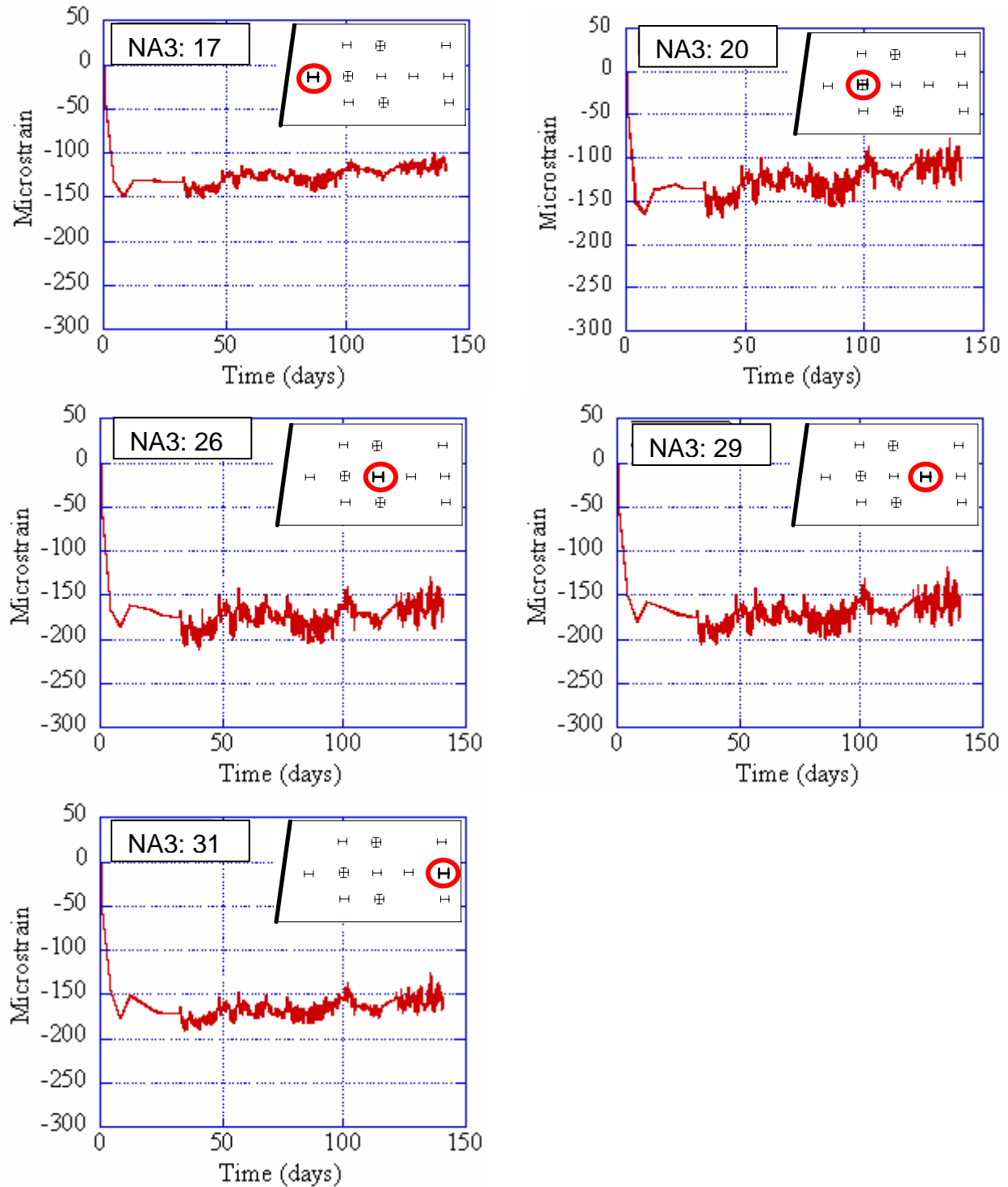


Figure 34. Plots of shrinkage for sensors in the middle of the lane, NA-LN-3 (From-11/01/02-03/14/03)

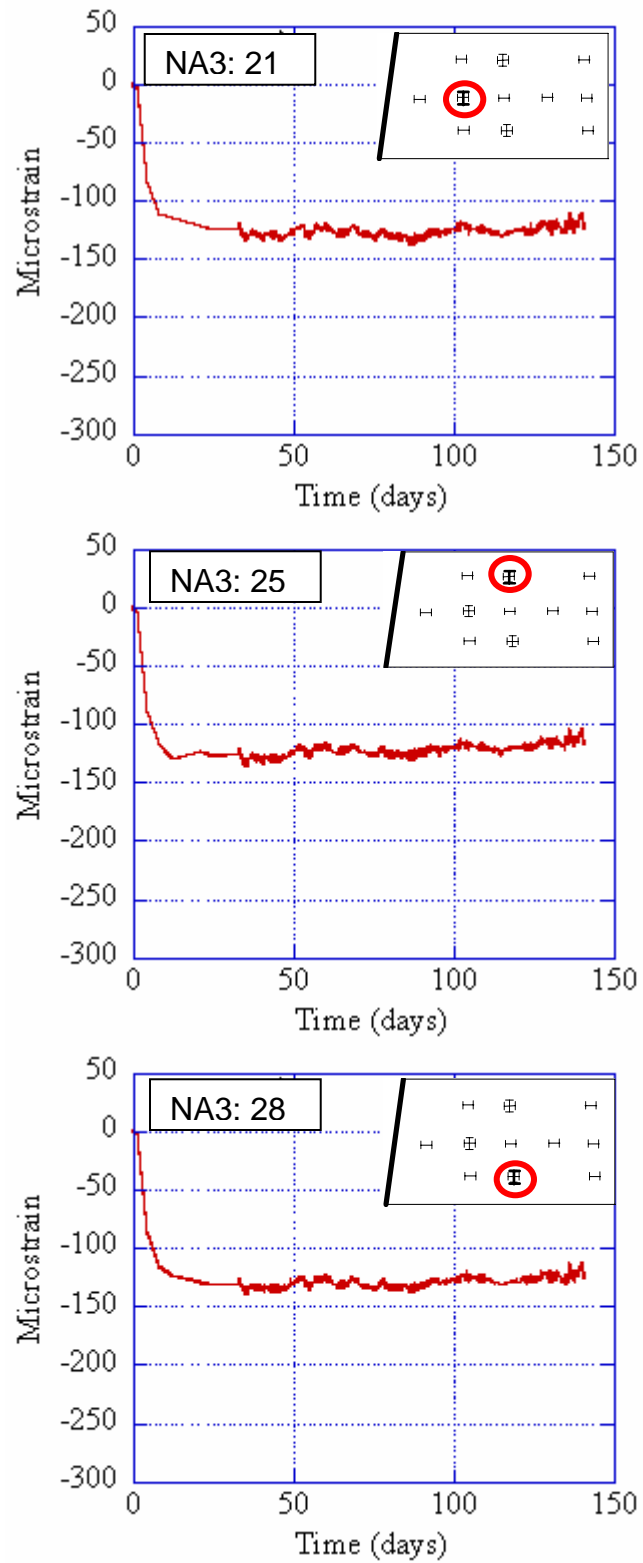


Figure 35. Plots of shrinkage for all transverse sensors, NA-LN-3. (From-10/24/02-03/14/03)

#### **VWSG Results from NA-LN-4.**

1. Concreting of NA-LN-4 was executed in second pour.
2. Figure 36 shows plots of shrinkage along the edge of the slab, which is towards the shoulder. Most of the sensors are showing same value of shrinkage. This makes sense because that edge of slab is restrained by shoulder.
3. Figure 37 shows plots of shrinkage along the edge of the slab, which is towards the NA-LN-3. Most of the sensors are showing same value of shrinkage. This makes sense because that edge of slab is restrained by shoulder.
4. Figure 38 shows plots of shrinkage along the middle edge of the slab. Most of the sensors are showing same value of strains. This makes sense because all are confined by concrete from both the sides.
5. Figure 39 shows plots of shrinkage for all transverse sensors. Transverse sensors are showing less shrinkage than longitudinal sensors. This makes sense because length is smaller in that direction.

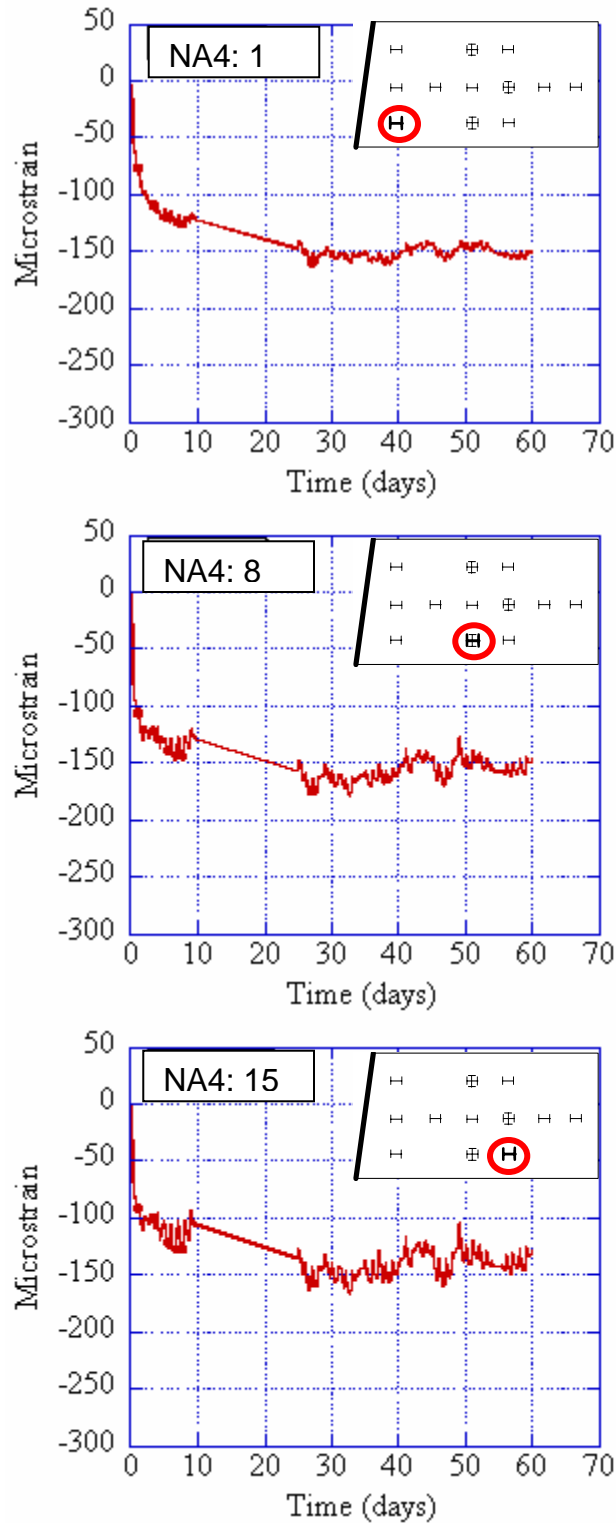


Figure 36. Shrinkage plots for sensors along edge towards shoulder (NA-LN-4). (From-11/01/02-03/14/03)

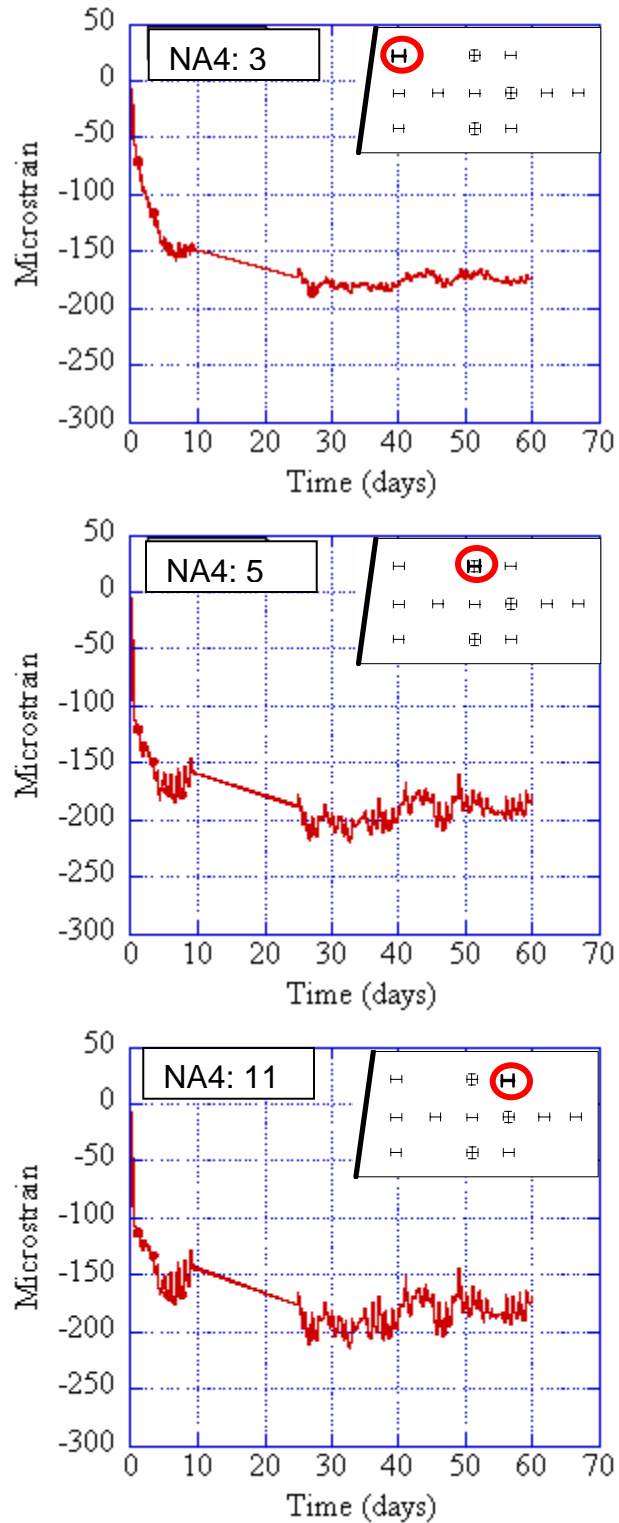


Figure 37. Shrinkage plots for sensors along edge towards NA-LN-3. (NA-LN-4). (From-11/01/02-03/14/03)

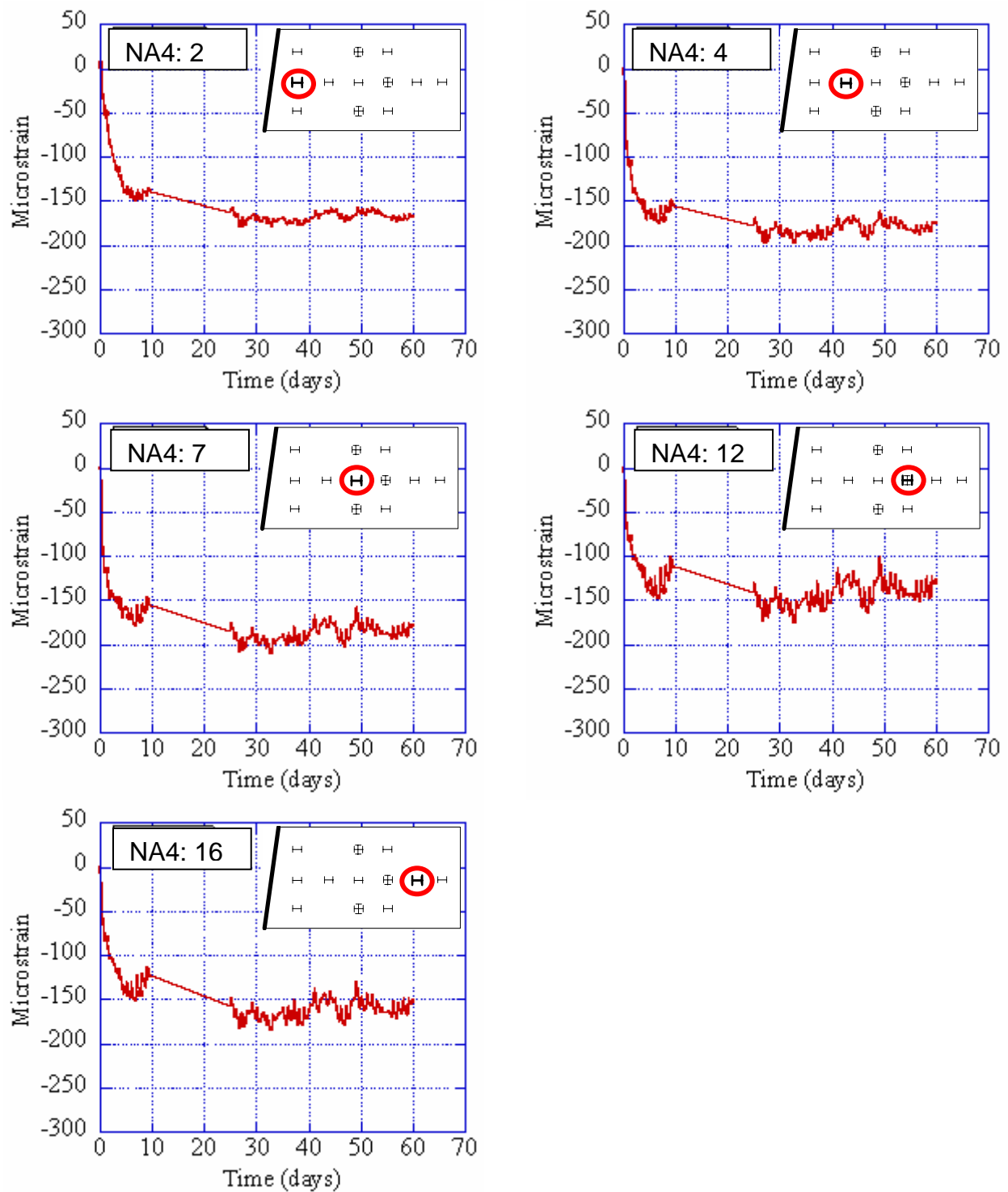


Figure 38. Plots of shrinkage for sensors in the middle of the lane, NA-LN-4 (From-11/01/02-03/14/03)



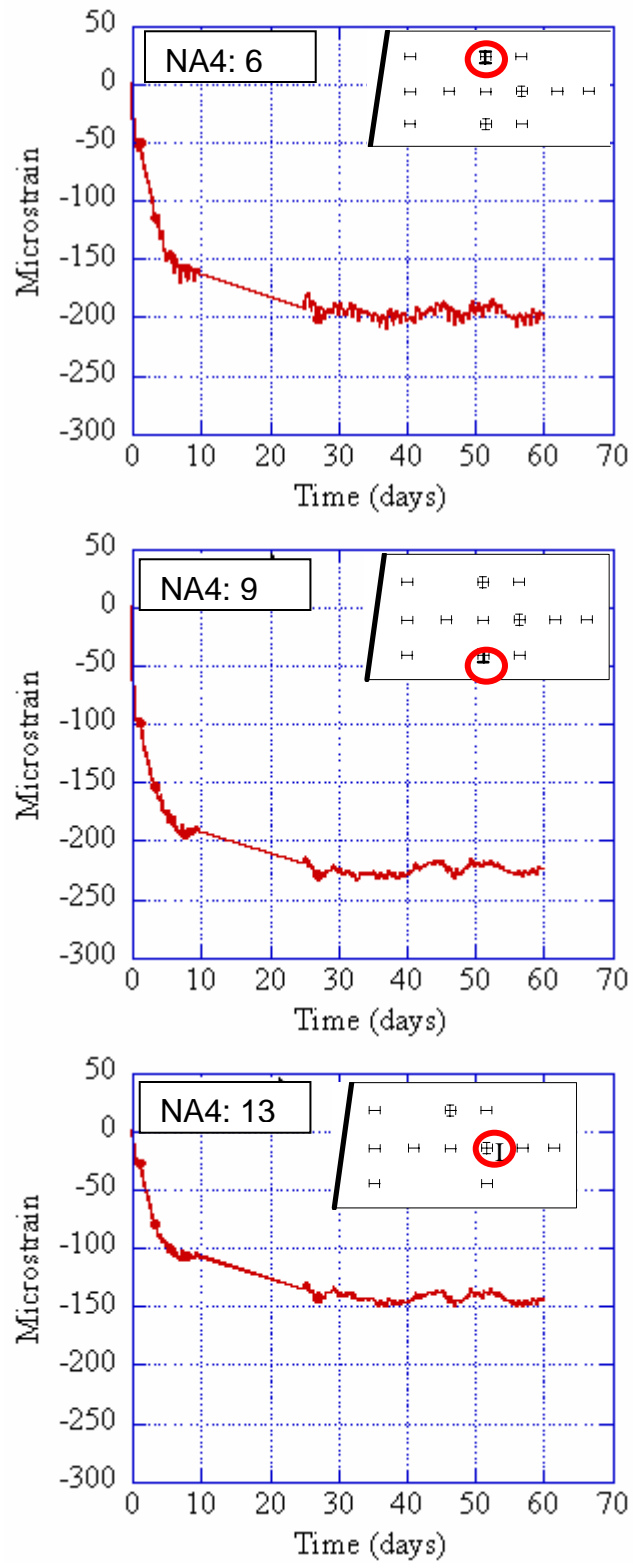


Figure 39. Plots of shrinkage for all transverse sensors, NA-LN-4. (From-10/24/02-03/14/03)

### **VWSG Results from SA-LN-3.**

1. Concreting of SA-LN-3 was done in second pour.
2. Figure 40 shows plots of shrinkage along the edge of the slab, which is towards SA-LN-4. Sensor nearer to abutment is showing less shrinkage than sensor that is farthest from the abutment. This makes sense, because sensor near to abutment has got sort of restrain in the abutment direction, while sensor away from abutment is free to shrink since there is nothing on the end.
3. Figure 41 shows plots of shrinkage along the edge of the slab, which is away from SA-LN-4. Sensor near and far from abutment are showing almost same strain. This makes sense, because concreting of SA-LN-4 was done first and this edge is restrained from that side.
4. Figure 42 shows plots of shrinkage along the middle edge of the slab. All sensors are showing same value of strains since they are confined by concrete from both sides.
5. Figure 43 shows plots of shrinkage for all transverse sensors. Sensors placed in the transverse direction are showing less shrinkage than those in the longitudinal direction since their length is smaller in the transverse direction.

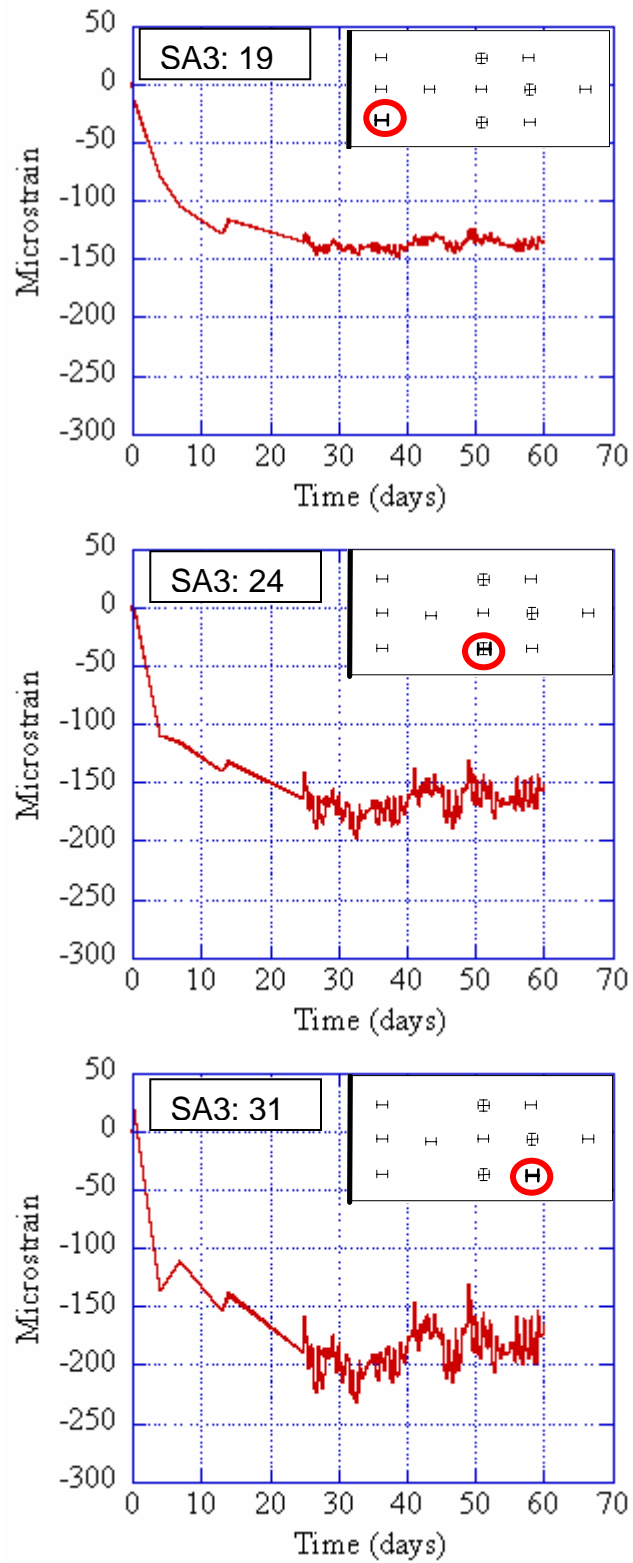


Figure 40. Shrinkage Plots for Edge Sensors towards SA-LN-4. (SA-LN-3) (From-10/24/02-03/14/03)

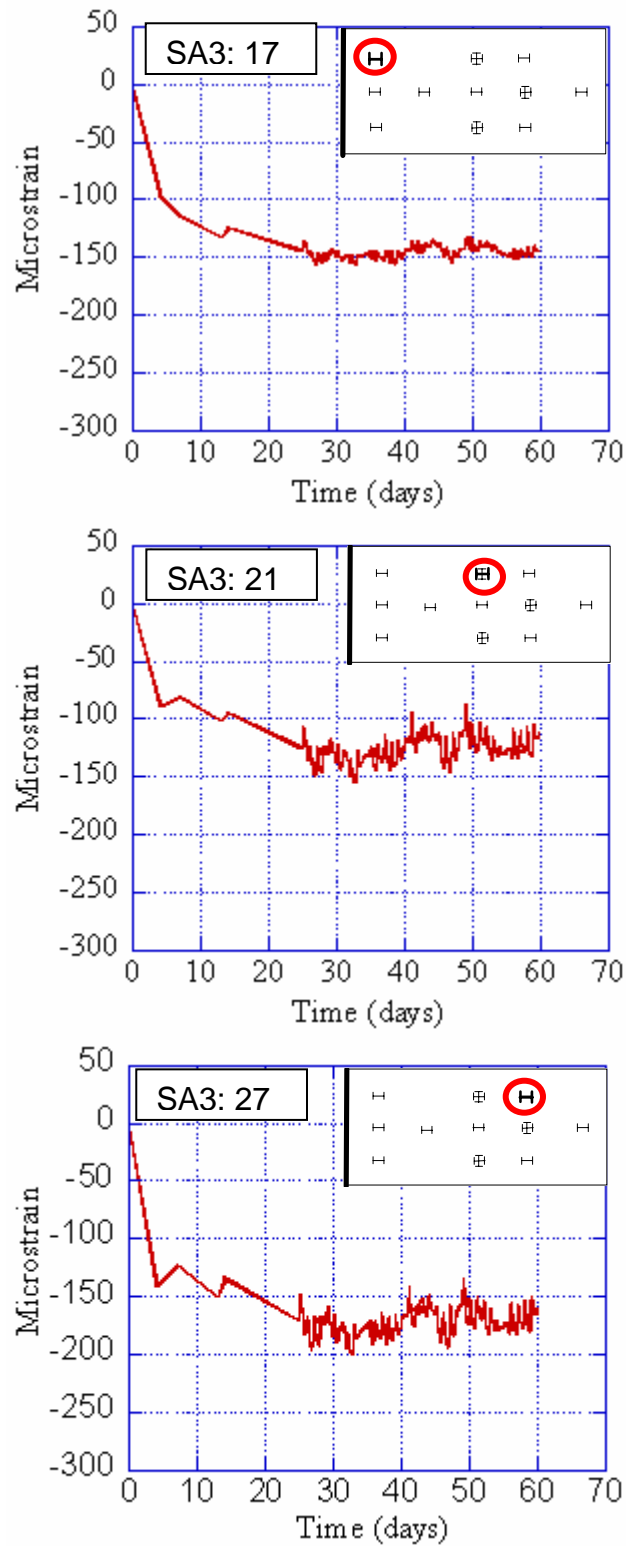


Figure 41. Shrinkage plots for sensors along edge away from SA-LN-4. (SA-LN-3)  
(From-10/24/02-03/14/03)

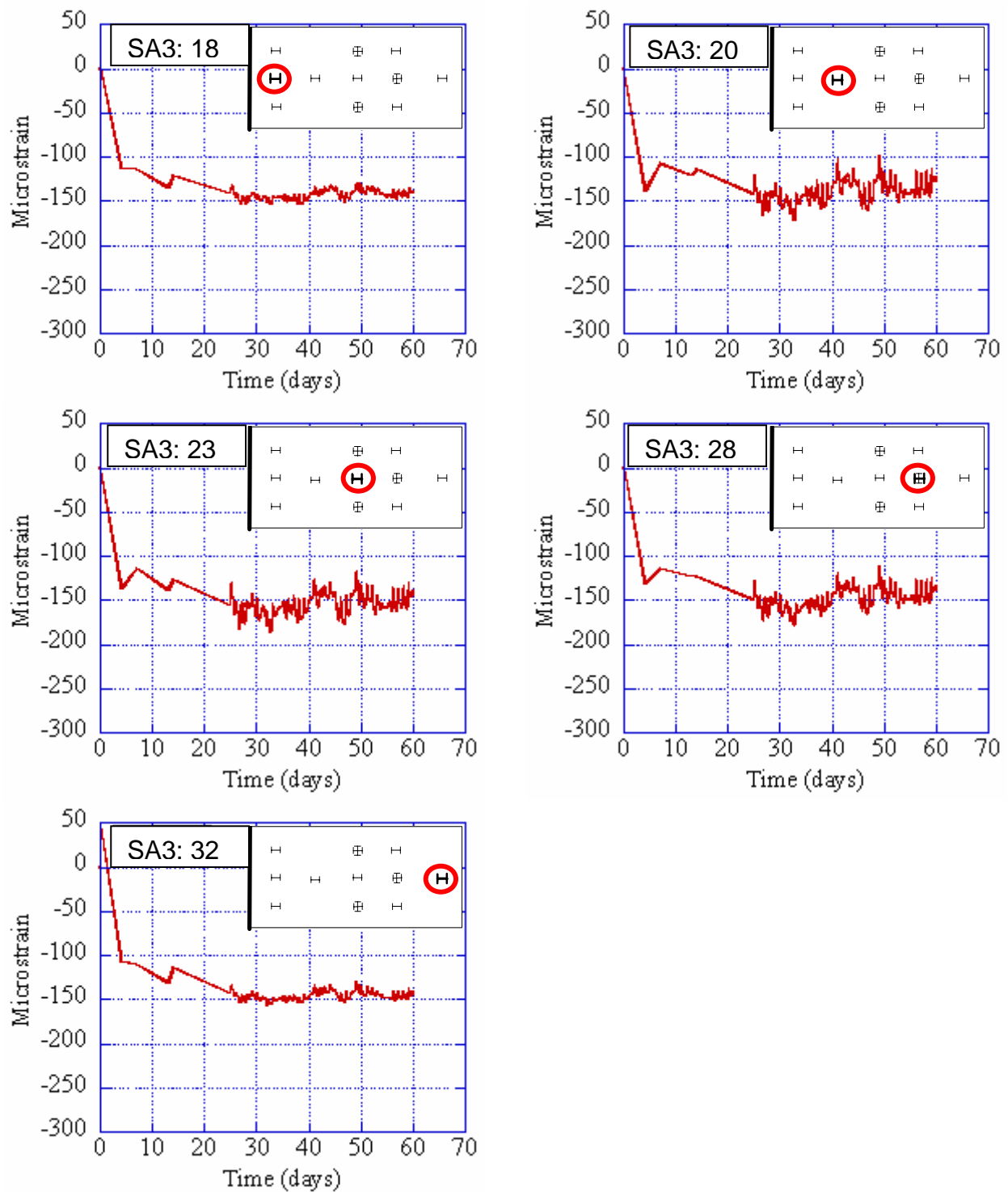


Figure 42. Plots of shrinkage for sensors in the middle of the lane, SA-LN-3 (From-11/01/02-03/14/03)

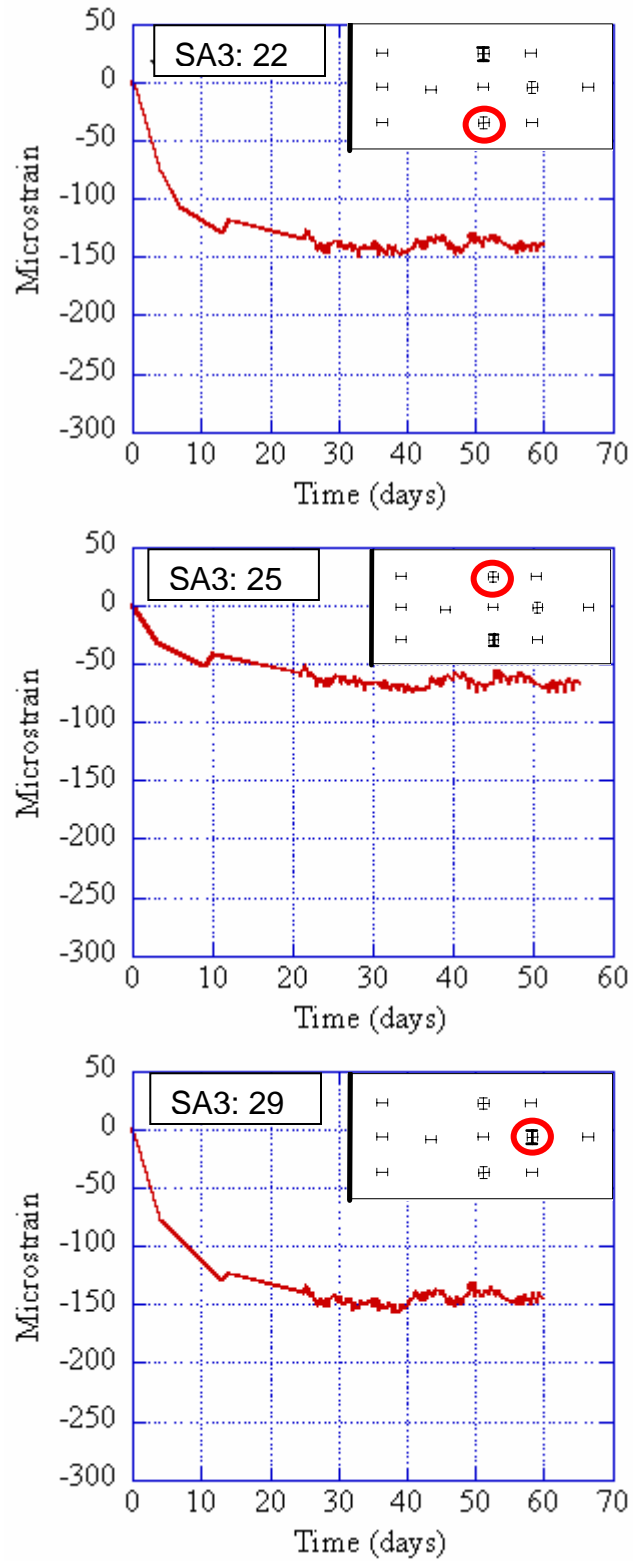


Figure 43. Shrinkage plots for all transverse sensors, SA-LN-3. (From-11/01/02-03/14/03)

#### **VWSG Results from SA-LN-4.**

1. Concreting of SA-LN-4 was done in first pour.
2. Figure 44 shows plots of shrinkage along the edge of the slab, which is away from SA-LN-3. Sensor nearest to the abutment is showing less shrinkage than those in the middle of the slab.
3. Figure 45 shows plots of shrinkage along the edge of the slab, which is towards SA-LN-3. Sensor nearest to the abutment is showing less shrinkage than sensors placed in the middle of the slab.
4. Figure 46 shows plots of shrinkage along middle edge of the slab. Most of the sensors are showing same value of strains since all of them are confined by concrete from both the sides.
5. Figure 47 shows plots of shrinkage for all transverse sensors. Sensors placed in the transverse direction are showing less shrinkage than those in the longitudinal direction since their length is smaller in the transverse direction.

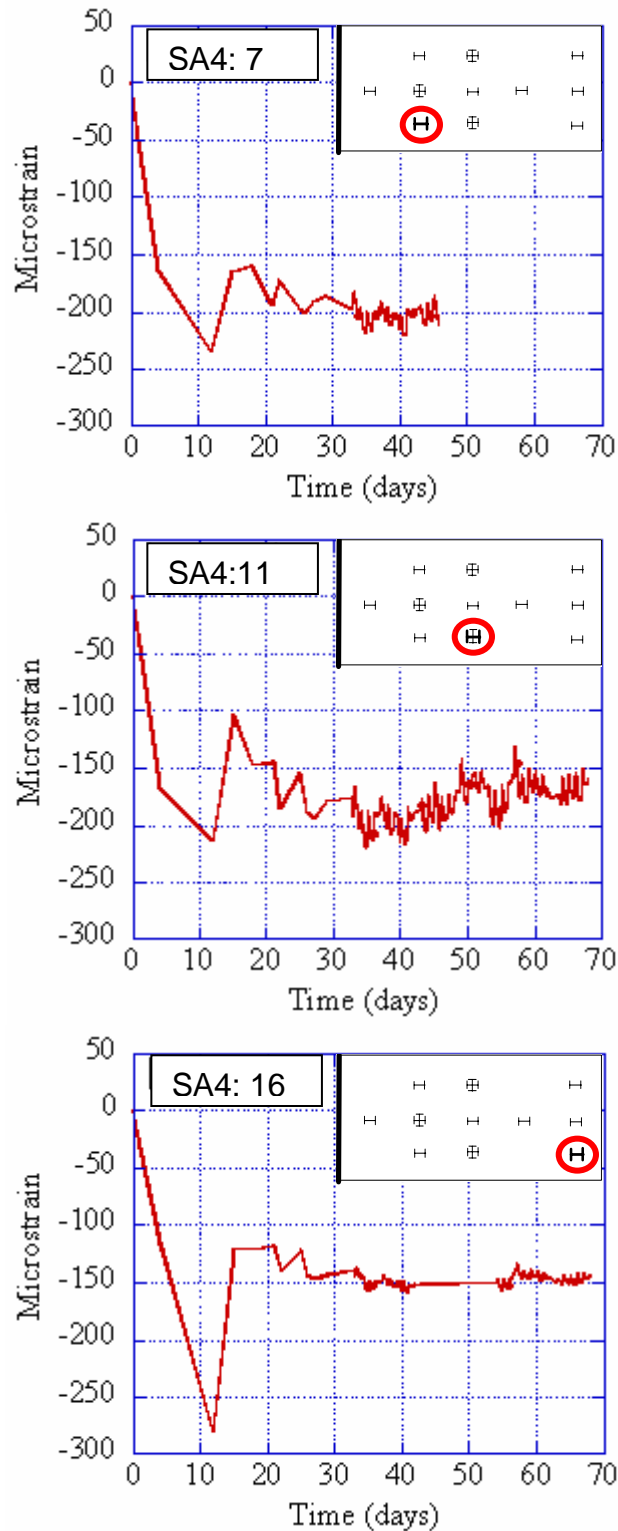


Figure 44. Shrinkage plots for sensors along edge towards shoulder. (SA-LN-4). (From-10/24/02-03/14/03)



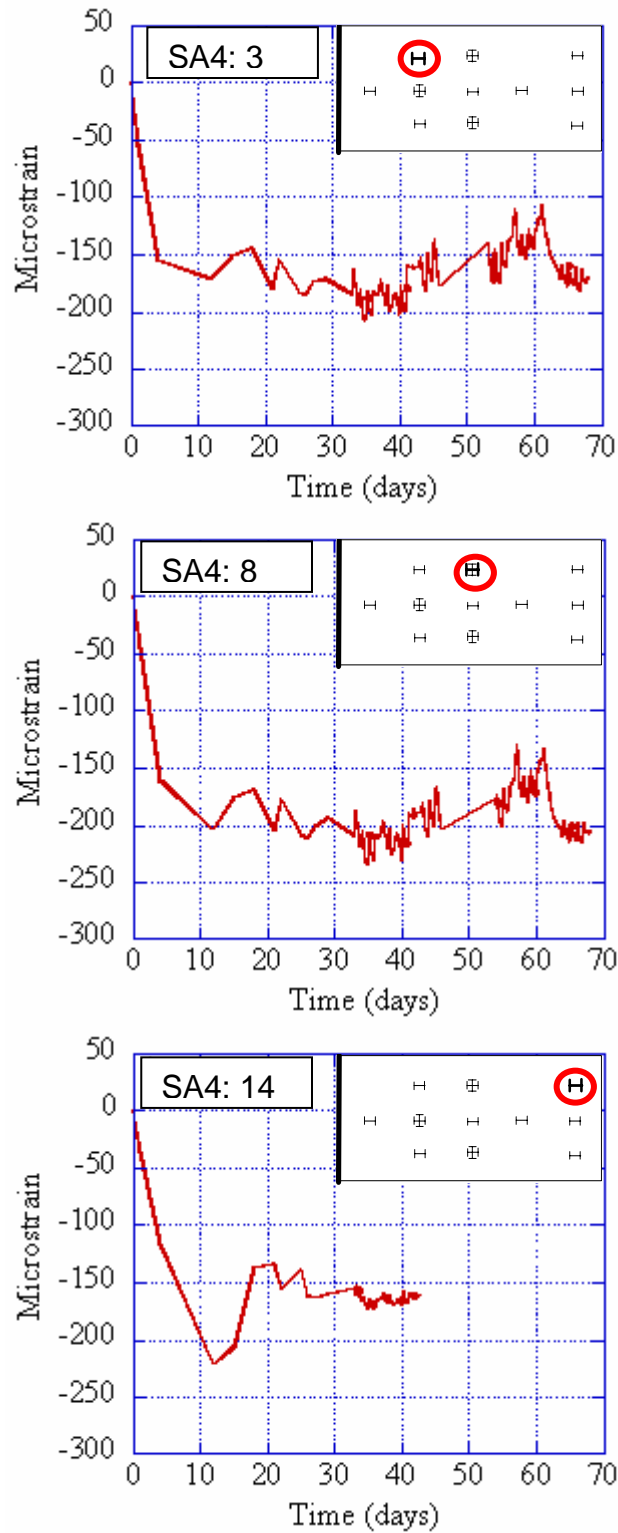


Figure 45. Shrinkage plots for sensors along edge towards SA-LN-3. (SA-LN-4). (From-10/24/02-03/14/03)

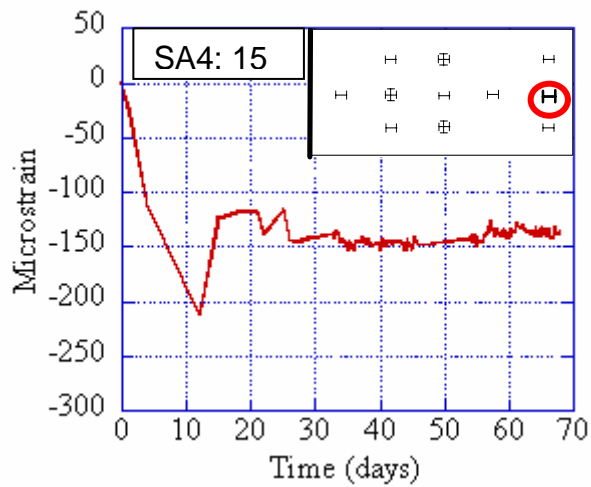
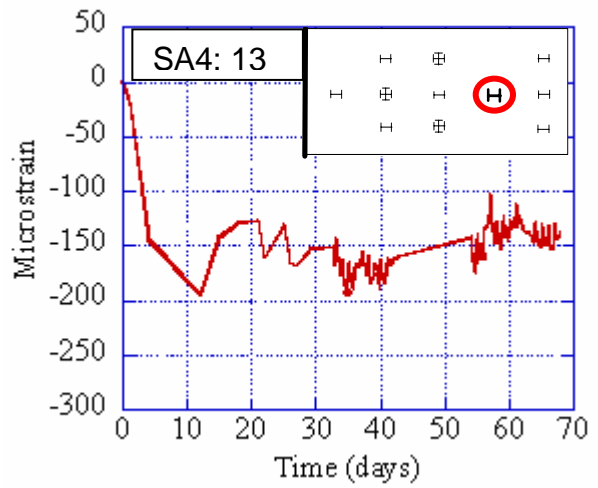
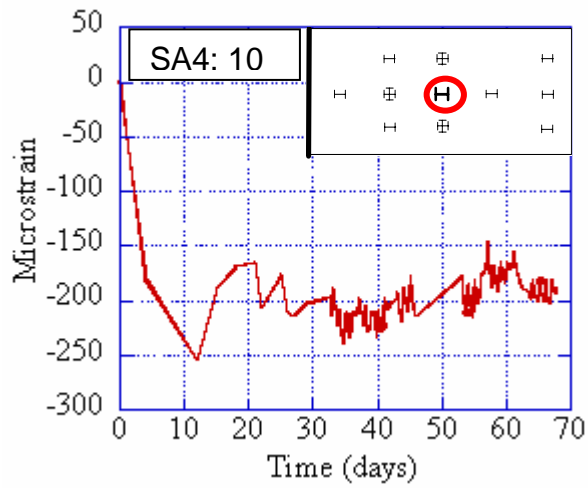
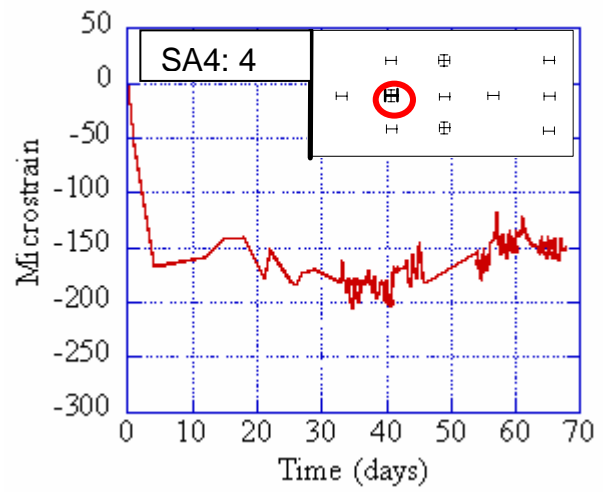
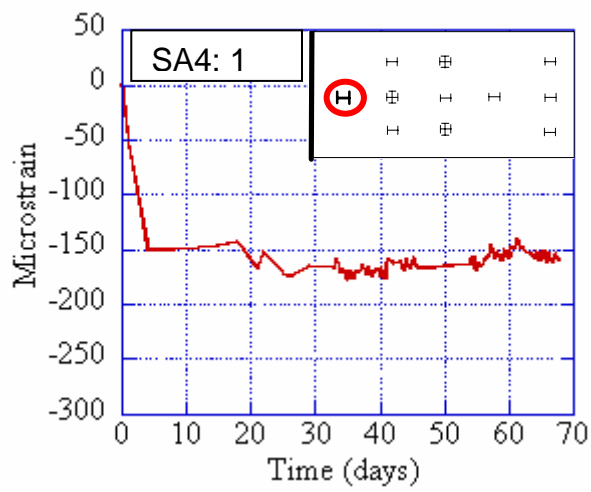


Figure 46. Plots of shrinkage for sensors in the middle of the lane, SA-LN-4. (From-10/24/02-03/14/03)

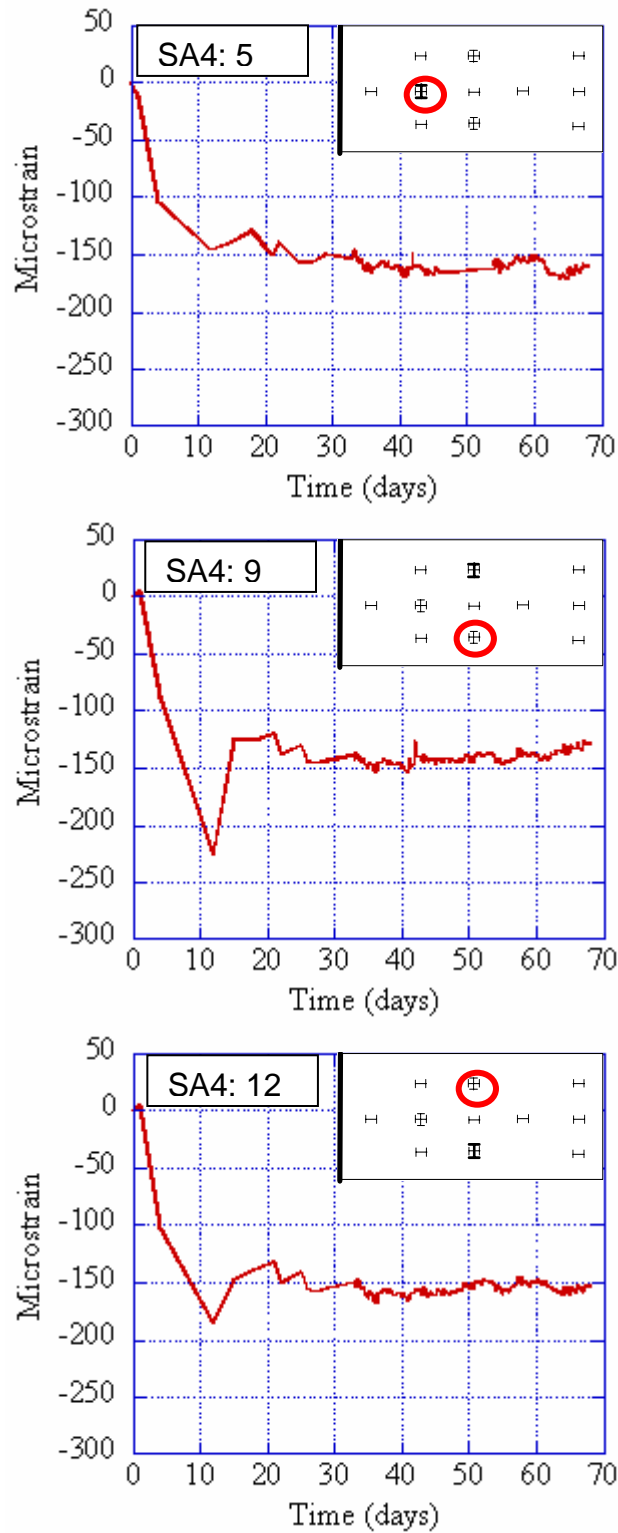


Figure 47. Shrinkage plots for transverse sensors, SA-LN-4. (From-10/24/02-03/14/03)

## Study of VW Deformation Data And Pressure Cell Data

Figure 48 shows a plot of deflection ( i.e., vertical movement) vs. time for SA-LN-3. The sensor away from the abutment is showing higher deflection in comparison to other sensors. This portion of the soil is not confined by the wing wall which allows for larger deflection.

Figure 49 (a) and (b) shows plots of available pressure cell data for SA-LN-3 and NA-LN-4. Pressure in these two sensors are different, because results depend on the type of soil contact with the pressure cell plate, concrete strength, etc, which are not the same for both the slabs.

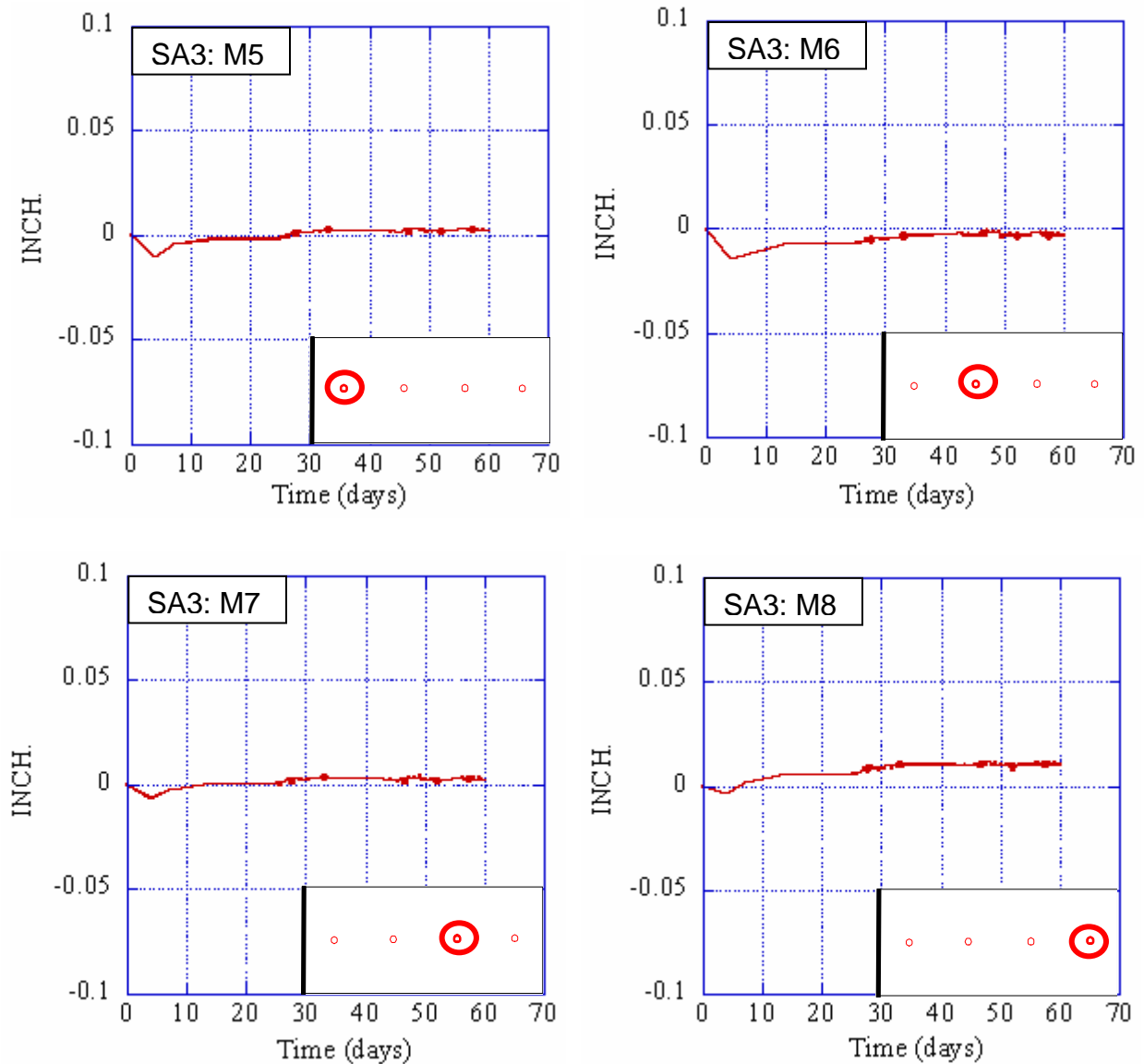
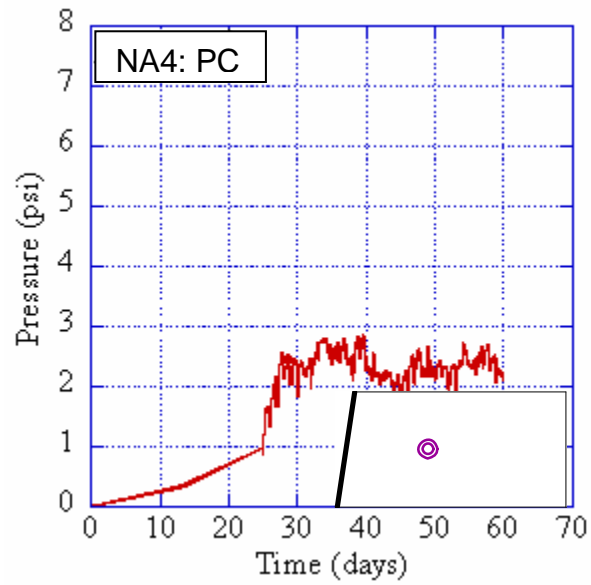
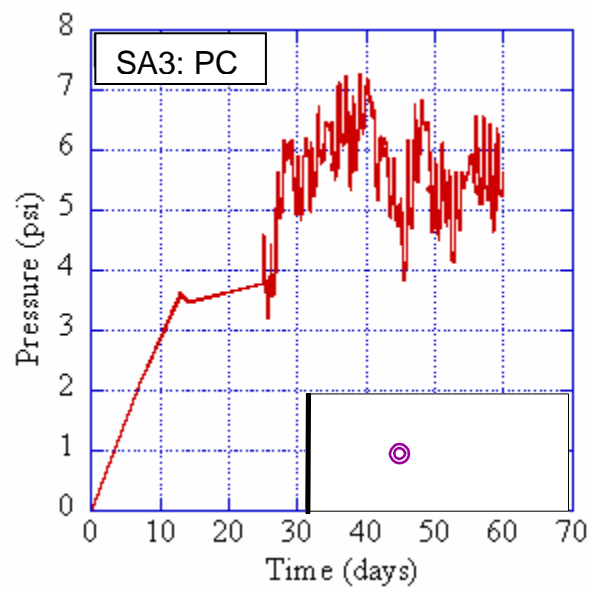


Figure 48. Plots of VW Deformation Meter for SA-LN-3. (From-11/01/02-12/31/02)



(a) NA-LN-4



(b) SA-LN-3

Figure 49. Plots for pressure cell data. (NALN-4 and SA-LN-3) (From-11/01/02-12/31/02)

## LONG-TERM MONITORING

The long-term behavior of the new design alternatives is also observed using the instrumented slabs on the Doremus Avenue Bridge. Figure 50 and Figure 51 illustrate typical strain readings of the proposed approach slabs in north and south abutments, respectively. The strain readings are taken from the VWSGs that are installed at the bottom reinforcement layer in the middle of the slab. Similar strain readings are observed in other locations where the slab expands and contracts but did not exhibit any cracking.

Figure 52 shows the approach slabs located at the south abutment of the Doremus Avenue Bridge and the weigh-in-motion (WIM) system installed in each traffic lane. Figure 52 also shows a crack that has occurred and developed during concreting of the SA-LN-1 approach slab due to cold joints and delay in delivering concrete on time. The behavior of each slab was recorded using the various sensors installed to monitor their long-term behavior. Figure 53 indicates the strain response when the concrete cracks. The cracks were observed as early as 14 days while the strain reading indicates that the same crack was initiated at 140 days. This can be explained by the fact that the VWSG was installed in the bottom rebar mat and the crack was propagating deeper over time.

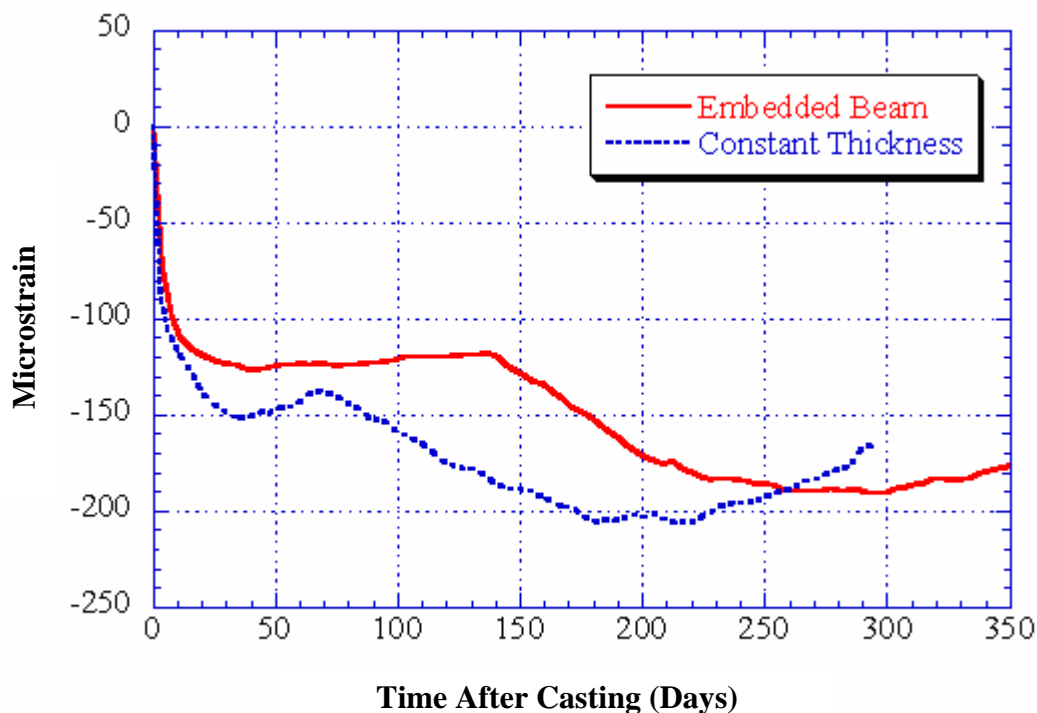


Figure 50. Typical Strain Readings of the EB and CT slabs in the North Abutment

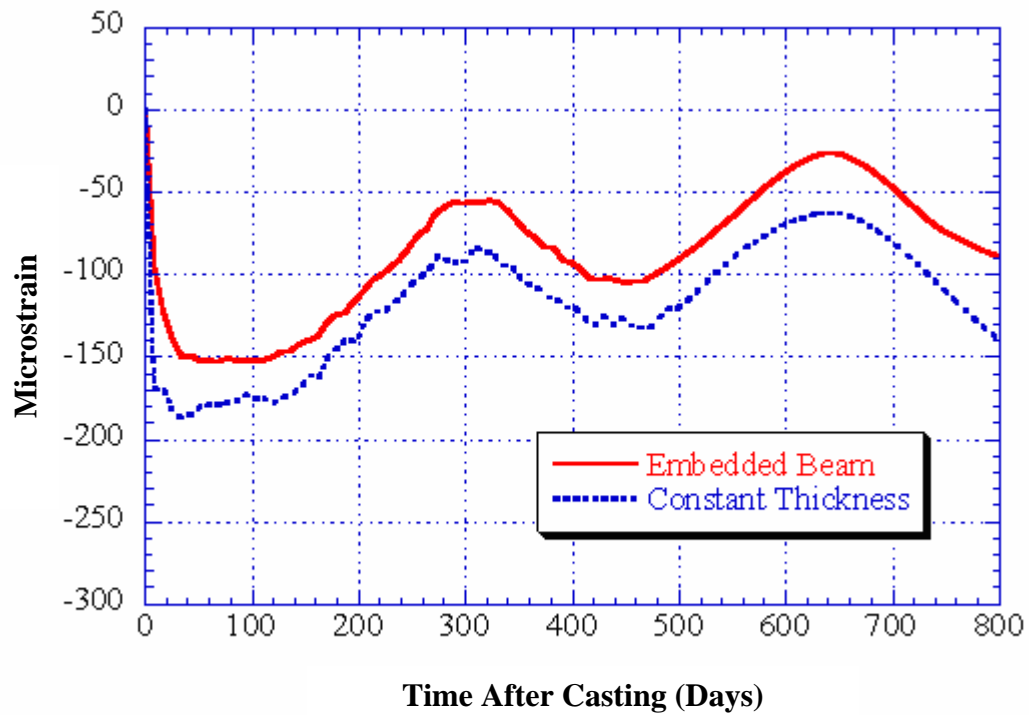


Figure 51. Typical Strain Readings of the EB and CT slabs in the South Abutment



Figure 52. Crack Location and orientation in new Approach Slab at the Doremus Avenue Bridge

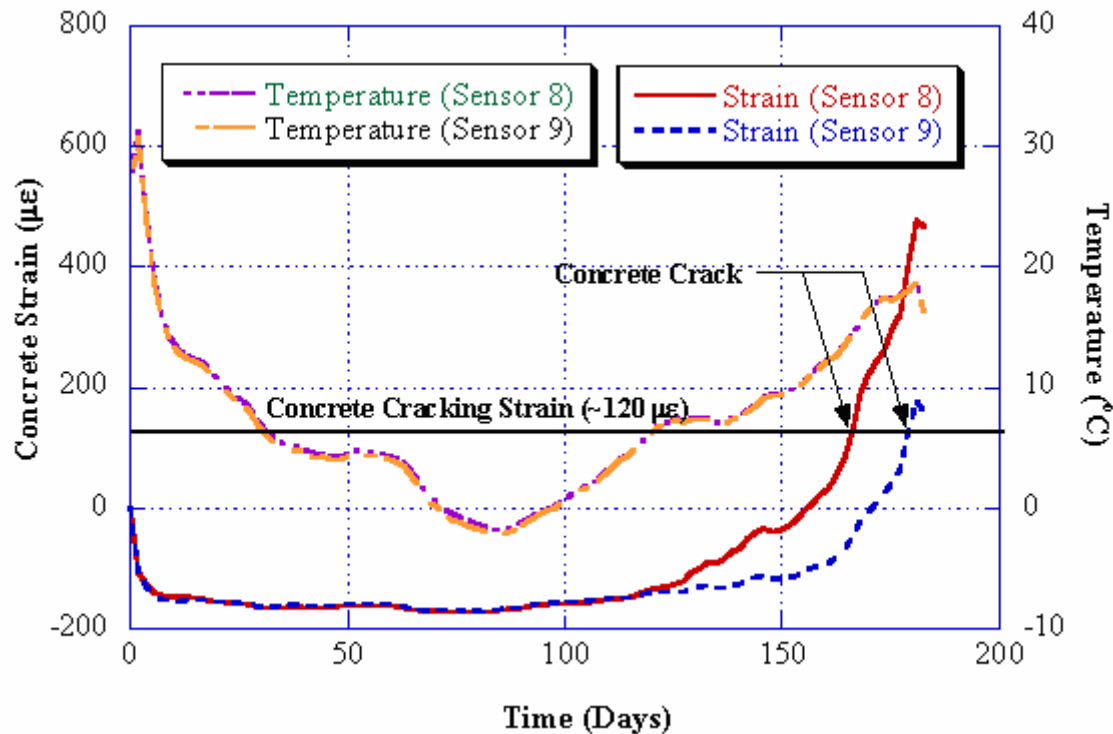


Figure 53. Strain and temperature profile at crack location.

Figure 54 illustrates a typical measured strain and temperature profile of the approach slab. It is observed that the concrete shrinks rapidly in the first 28 days and then the strain is stabilized. It is also shown that as the temperature rises the concrete expands. The data also confirmed field observation since there were no cracks observed at this location. Figure 55 shows the displacement and pressure between the concrete slab and the top of the soil at the same location. It is observed that there is no significant movement between soil and the slab while relatively small pressure changes are expected because of slab curling. As the concrete shrinks in the first 28 days, the concrete curled and lost contact with the soil causing the contact pressure to drop. As the concrete stops shrinking, the pressure increases. Hence, it could be concluded that there is no settlement problem in the slab.

Furthermore, the EB design alternative was also adopted for Route 35 Victory Bridge that connects Port Amboy, NJ to Sayreville, NJ after multiple cracks were observed on the transitional slabs because the abutment wing needed for hugging the soil cannot be constructed until Stage II construction preventing the compaction of the soil.



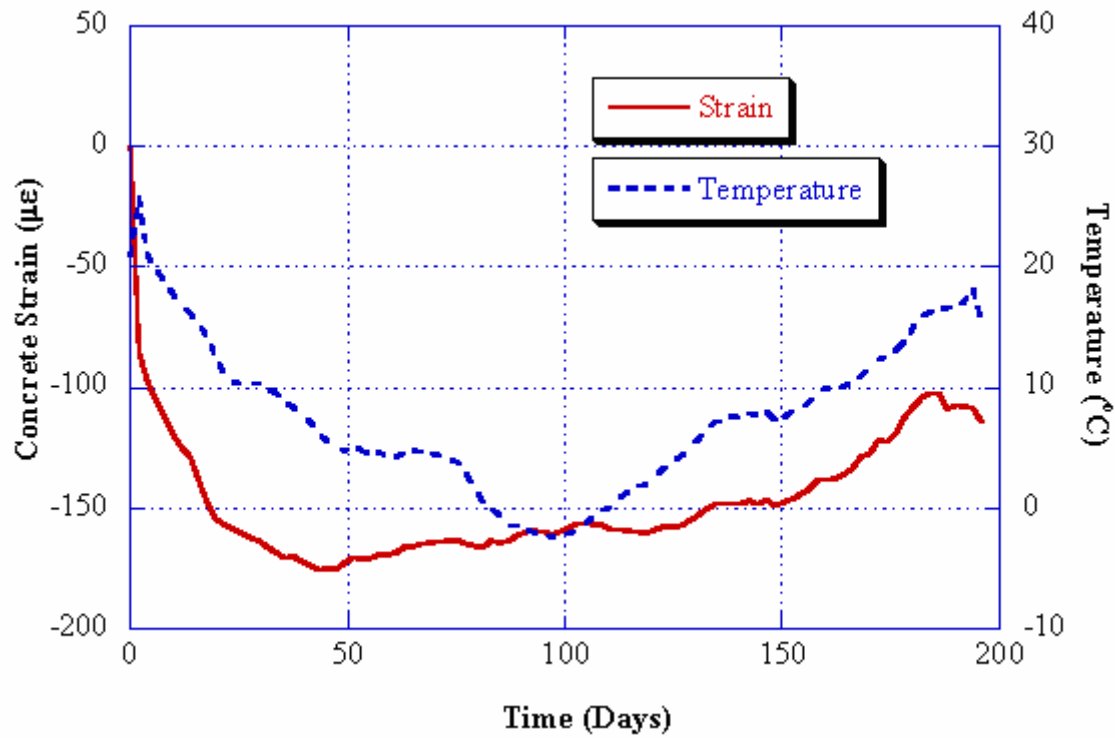


Figure 54. Typical strain and temperature profile of approach slabs.

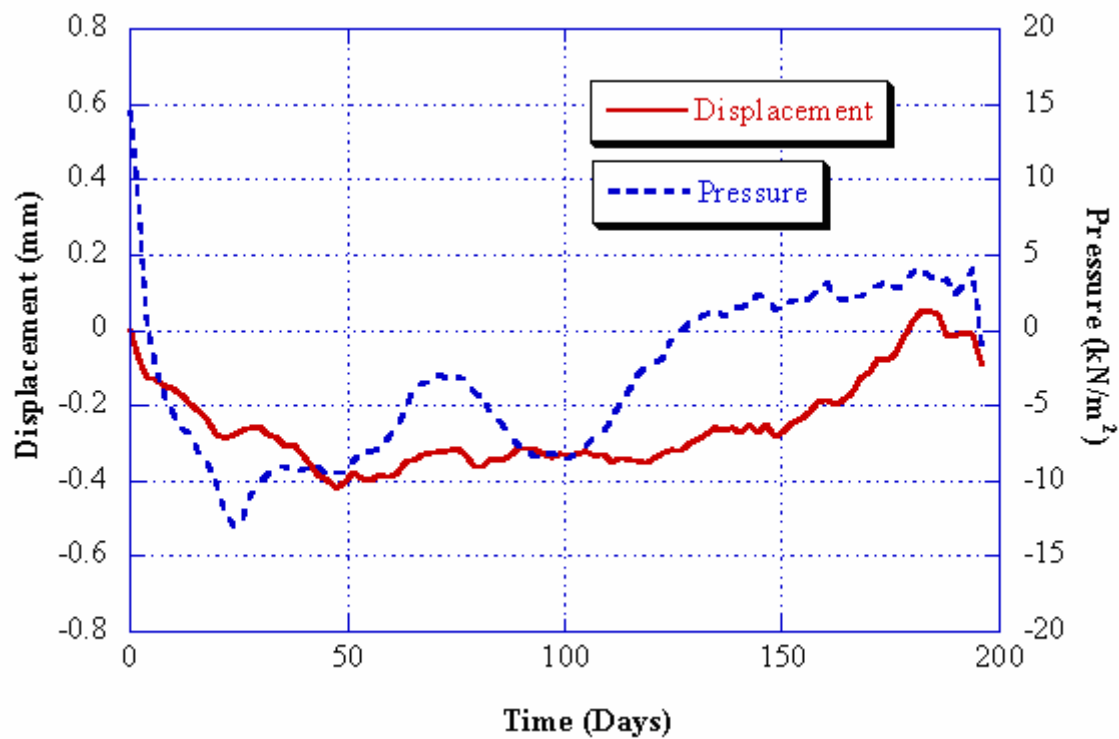


Figure 55. Typical displacement and pressure profile of approach slabs.

## **CONCLUSIONS**

The following conclusions can be made:

1. Embedded beam (EB) design alternative provides the best performance based on results from the FE analysis, static load testing, and long-term monitoring performance. None of the EB approach slabs that were properly constructed exhibited any cracks under normal truck traffic conditions or soil settlement.
2. The existing 3D finite element model gives accurate prediction of the strains in the approach slabs in comparison with actual measurements from the vibrating wire strain gages.
3. Long-term monitoring of the construction of the approach slab provides significant information of the construction process, design assessment, and failure detection. The sensors were successfully used in detecting construction problems at two occasions: (1) premature loading and (2) development of cold joints.
4. Over the period of the long term monitoring (e.g., 2 years), there is no significant amount of settlement in the soil underneath approach slab.
5. A 35ft and 45ft slab has the capacity to take 4.5 HS20, while a 55ft slab has a load carrying capacity of 4.3 HS20.
6. The 45 ft length was the optimum design length without increasing the cost of the approach slabs.

## **RECOMMENDATIONS**

The following recommendations can be made:

1. Adopt the EB design alternative as the detail for the NJDOT new design of approach slabs.
2. Eliminate transition slabs, i.e. adopt approach slabs with 18" constant thickness.
3. Ensure proper compaction of the backfill material below the approach slab since it is extremely important in minimizing settlement.
4. Extend the length of the wing wall beyond the current practice of 25-30 feet to minimize embankment bulging.
5. Continue to monitor the performance of the approach slabs for a longer period of time (i.e., beyond the current duration of the project) to allow for the observation of any soil settlement or embankment bulging and their effects.

## REFERENCES

1. Nassif, H., Abu-Amra, T., and Shah, N. "Finite Element Modeling of Bridge Approach and Transition Slabs," Report FHWA NJ 2002-007, New Jersey Department of Transportation, 2002.
2. Khodair, Y. "Finite Element Modeling of Bridge Approach Slabs", MS Thesis, Department of Civil and Environmental Engineering, Rutgers University, October 2001.
3. Khodair, Y. and Nassif, H. "Finite Element Analysis of Bridge Approach Slabs Considering Soil-Structure Interaction," Journal of Bridge Structures, Vol. 1, No. 3, 2005, pp. 245-256.
4. Briaud, J. L., James, R. W. and Hoffman, S. B. "TRB, NCHRP Synthesis of Highway Practice 234: Settlement of Bridge Approaches Bump at the End of the Bridge". National Academy Press, Washington, D.C. 1997.
5. Ardani, A. Bridge Approach Settlement: Report No. CDOH-DTP-R-87-6, Colorado Department of Highways, April 1987.
6. Bathe, Klaus J. and Wilson, Edward L.: Numerical Methods in Finite Element Analysis. Prentice Hall Inc., 1976.
7. Bowels, Joseph E.: Foundation Analysis and Design. Fifth Edition, McGraw-Hill, Inc, 1996.
8. Burnett, David S.: Finite Element Analysis: From Concepts to Applications. Addison-Wiley Publishing Company, AT&T Bell Laboratories.
9. Gere, James M. and Timoshenko, Stephen P.: *Mechanics of Materials*. PWS Publishing Company, 1997.
10. Nawy, Edward G.: Reinforced Concrete A Fundamental Approach. Fourth Edition, Prentice Hall International, New Jersey, 2000.
11. "Integral abutment and jointless bridges," Structural Engineer, Federal Highway Administration, Washington DC, by V. C. Mistry.
12. "Integral abutment bridges: Problems and Innovative solutions" Manhattan College Research Report No. CE/GE-00-2.
13. Schaefer, Vernon R and Koch, Jay C.; Void Development under Bridge Approaches: Final Report No SD90-03. South Dakota Department of Transportation, November 1992.

14. Wolde-Tinsae, A.M., Greiman, L.F.; and Johnson B., "Performance of Integral Bridge Abutments," Journal of the International Association for Bridge and Structural Engineering, IABSE Periodical 1/1983, February 1983.
15. Wolde-Tinsae, A.M, Aggour, S.M; and Chini; S.A. Structural and Soil Provisions for Approaches to Bridges: Interim Report AW087-321-046, Maryland Department of Transportation July 1987.
16. NCHRP, Synthesis of Highway Practice 159, "Design and Construction of Bridge Approaches." Transportation Research Board, National Research Council, Washington, D.C. 1990.
17. Huebner, Kenneth H.: The Finite Element Method for Engineers. John Wiley & Sons Inc. 1975.

## APPENDIX A

Details of the existing design of the approach slab, as provided by DOT, are shown in Figure 56 and Figure 58. Details of the EB design alternative adopted by NJDOT are shown in Figure 58.

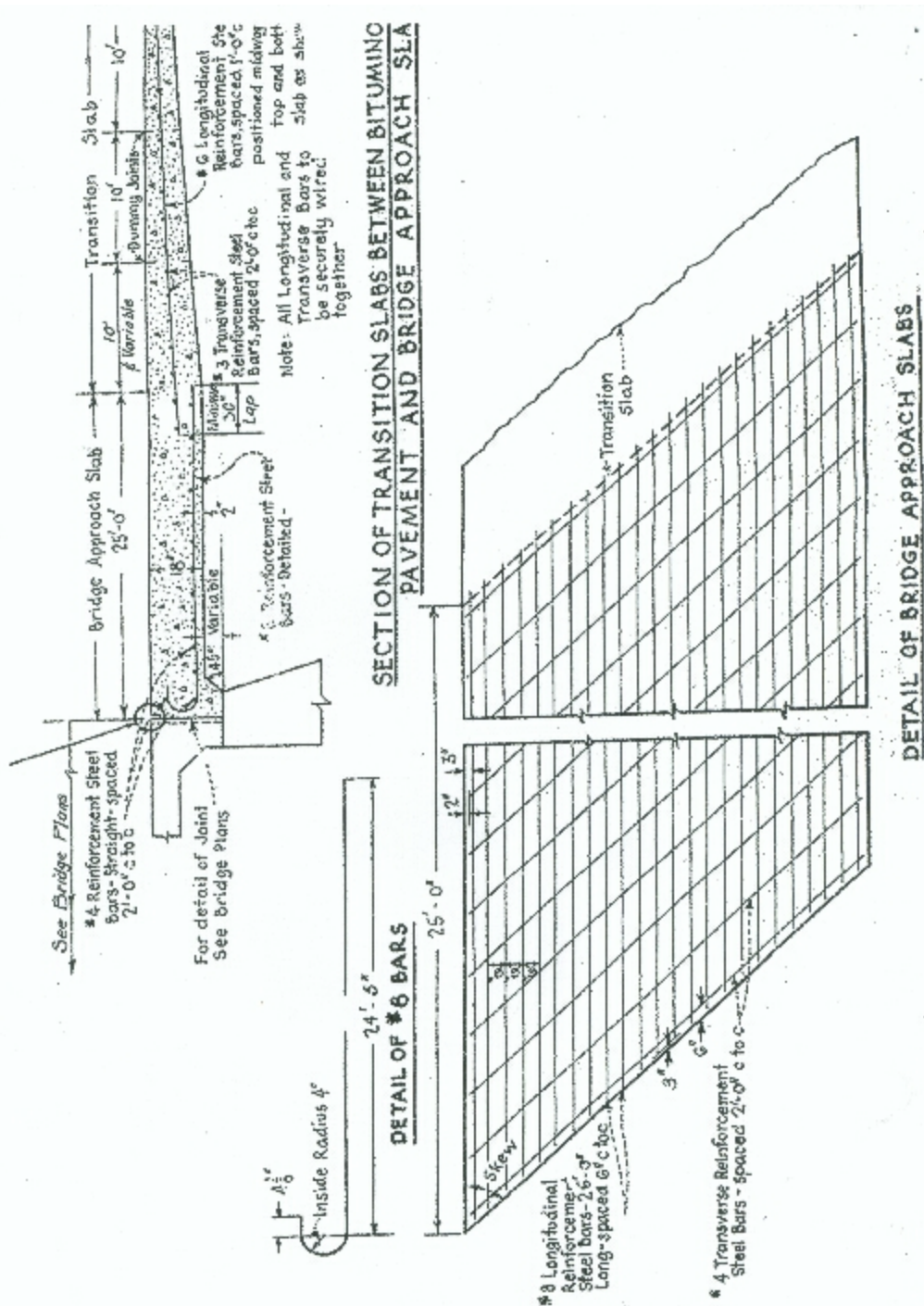


Figure 56. Detail of Existing Design of Approach Slabs.

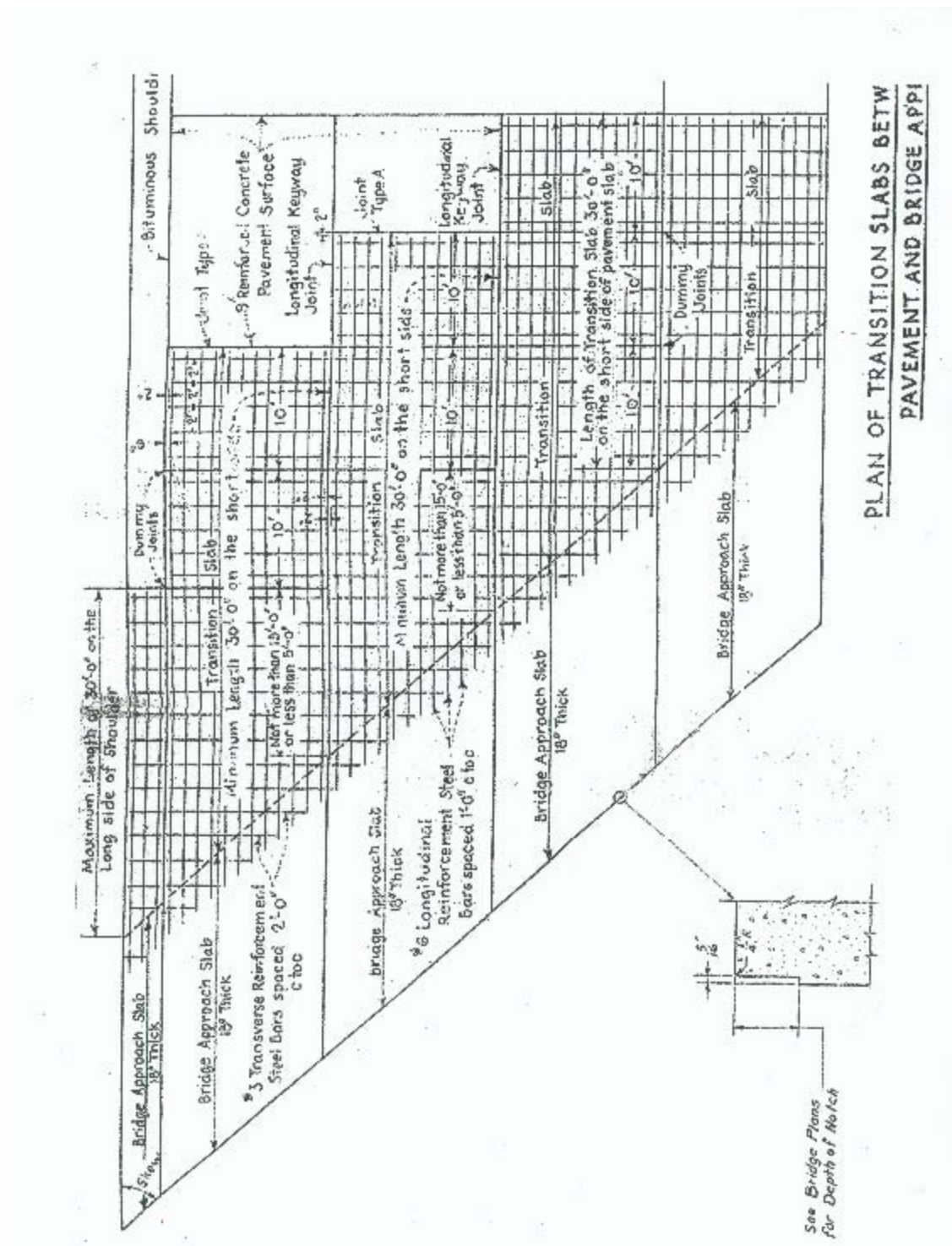


Figure 57. Detail of Existing Design of Transition Slabs.

